Downloaded from orbit.dtu.dk on: Apr 20, 2024

DTU Library

Wave-induced seabed residual response and liquefaction around a mono-pile foundation with various embedded depth

Sui, Titi; Zhang, Chi; Jeng, Dong-sheng; Guo, Yakun; Zheng, Jinhai; Zhang, Wei; Shi, Jian

Published in:
Ocean Engineering

Link to article, DOI:
https://doi.org/10.1016/j.oceaneng.2018.12.055

Publication date:
2019

Document Version
Peer reviewed version

Link back to DTU Orbit

Citation (APA):
Sui, T., Zhang, C., Jeng, D., Guo, Y., Zheng, J., Zhang, W., & Shi, J. (2019). Wave-induced seabed residual response and liquefaction around a mono-pile foundation with various embedded depth. *Ocean Engineering*, *173*, 157-173. https://doi.org/10.1016/j.oceaneng.2018.12.055

General rights
Copyright and moral rights for the publications made accessible in the public portal are retained by the authors and/or other copyright owners and it is a condition of accessing publications that users recognise and abide by the legal requirements associated with these rights.

- Users may download and print one copy of any publication from the public portal for the purpose of private study or research.
- You may not further distribute the material or use it for any profit-making activity or commercial gain
- You may freely distribute the URL identifying the publication in the public portal

If you believe that this document breaches copyright please contact us providing details, and we will remove access to the work immediately and investigate your claim.

*REVISED Manuscript UNMARKED
Click here to view linked References

Wave-induced seabed residual response and liquefaction around a mono-pile foundation with various embedded depth

Titi Sui[1, 2, 3], Chi Zhang[1, 2, *], Dong-sheng Jeng[1, 4], Yakun Guo[2, 5 *], Jinhai Zheng[1, 2], Wei Zhang[1, 2], Jian Shi[1, 2]

[1]*State Key Laboratory of Hydrology-Water Resources and Hydraulic Engineering, Hohai University, Nanjing, Jiangsu 210098, China*

[2]*College of Harbour, Coastal and Offshore Engineering, Hohai University, Nanjing, Jiangsu 210098, China*

[3]*Technical University of Denmark, Department of Mechanical Engineering, DK-2800 Kgs. Lyngby, Denmark*

[4]*School of Engineering and Built Environment, Griffith University Gold Coast Campus, Queensland 4222, Australia.*

[5]*Faculty of Engineering and Informatics, University of Bradford, Bradford, BD7 1DP, UK.*

Corresponding author: Chi Zhang; zhangchi@hhu.edu.cn

Yakun Guo; y.guo16@bradford.ac.uk

Abstract: Wave-induced seabed instability caused by the residual liquefaction of seabed may threaten the safety of an offshore foundation. Most previous studies have focused on the structure that sits on the seabed surface (e.g., breakwater and pipeline), a few studies investigate the structure embedded into the seabed (e.g. a mono-pile). In this study, by considering the inertial terms of pore fluid and soil skeleton, a three-dimensional (3D) integrated model for the wave-induced seabed residual response around a mono-pile is developed. The model is validated with five experimental tests available in the literature. The proposed model is then applied to investigate the spatial and temporal pattern of pore pressure accumulation as well as the 3D liquefaction zone around a mono-pile. The numerical simulation shows that the residual pore pressure in front of a pile is larger than that at the rear, and the seabed residual response would be underestimated if the inertial terms of pore fluid and soil skeleton are neglected. The result also shows that the maximum residual liquefaction depth will increase with the increase of the embedded depth of the pile.

Keywords: Wave loading; seabed residual response; inertial terms; pile foundation; embedded depth; liquefaction.

1. Introduction

Offshore marine structures are normally subjected to complex dynamic environmental loadings during their service lifetime (Sumer, 2014). Their operational safety affected by wave, current, tidal and seabed instability attracts the continuous attention of offshore engineers and researchers (e.g., Mattioli et al., 2012; Fuhrman et al., 2014; Zheng et al., 2014; Liang et al., 2015; Zhang et al. 2017; Zhang W. et al. 2018). A mono-pile has been widely used as the foundation of offshore wind power system, which occupies approximately 80% of the commonly-used structural types (e.g., gravity, tripods, and jacket) in the European market (EWEA, 2016). Regarding the failure of marine structure in an extreme hydrodynamic environment, it is believed that this may be due to the wave-induced seabed instability around foundations, rather than the construction deficiencies caused by wave impaction (Smith and Gordon, 1983). When a wave propagates over a seafloor, an excessive pore pressure within the seabed would be generated, particularly under a poor drainage condition of soil. If the excess pore pressure becomes greater than the overburden pressure, the resistance of soil skeleton will be fully lost owing to soil liquefaction, which threatens the stability of structures. This implies an accurate evaluation of the wave-induced seabed response is important in design of an offshore structural foundation.

Extensive studies have been conducted to investigate the wave-induced seabed response owing to its practical importance since the 1970s (Yamamoto et al., 1978). Based on the experiments and field observations (Zen and Yamazaki, 1990), two mechanisms for the wave-induced pore pressure variation can be identified, namely, an oscillatory mechanism and a residual mechanism. An oscillatory mechanism is usually found in the unsaturated sandy seabed with good drainage conditions, where a sharp upwardly directed pressure gradient may lead to the momentary seabed liquefaction (Madsen, 1978; Alcérreca-Huerta and Oumeraci, 2016; Zhou et al., 2018). In contrast, a residual mechanism can be observed in a silt seabed with low permeability. For the residual mechanism, the corresponding compaction of soil skeleton leads to an accumulated pore pressure, which promotes the seabed residual liquefaction. As reported in Jeng and Seymour (2007), residual mechanism will dominate the process of seabed liquefaction for poorly-drainage conditions. Note that, this study would focus on the wave-induced residual liquefaction of a seabed around a mono-pile.

Among the previous works for wave-induced residual liquefaction of seabed, Seed and Rahman (1978) may have been the first to investigate the pore pressure accumulation under wave loading. In their study, the cyclic shear stress was taken into consideration using a non-linear source term for pore pressure accumulation. Using the approximate linear-relation of the source term, McDougal et al. (1989) proposed analytical solutions for the pore pressure accumulation for a shallow, medium, and deep seabed. The above solution was re-examined by Cheng et al. (2001) and some mistakes of mathematical derivationed were reported. In their study, an analytical solution using the Fourier transform was developed for the pore pressure accumulation. As pointed out by Jeng et al. (2007), some mistakes were made in both McDougal (1989) and Cheng et al. (2001). After correction of the previous work, the theoretical approach of Jeng et al. (2007) is shown to provide a better prediction. In their approach, Laplace

Transportation was used for deep foundation, while Fourier Transformation was sued for shallow foundation and a seabed of finite thickness. Based on the analytical solution, a simplified model for prediction for residual liquefaction (so-called J-S curve) was proposed in Jeng and Seymour (2007). Furthermore, as reported in Jeng et al. (2007), the predicated pore pressures based on both non-linear and linear-relations of the source term are almost identical. Therefore, no any further research is needed for considering the non-linear relations of the source term. Sumer et al. (2012) carried out a series of experimental tests to determine several empirical factors for the residual response of seabed. Using centrifuge flume tests, Sekiguchi et al. (1995) and Sassa and Sekiguchi (1999) examined the relationship between the elasto-plastic soil behaviour and pore pressure build-up. Their studies considered the conditions under loadings of both propagating and standing waves. Based on the residual model of Smits et al (1978), Meijers and Luger (2012), and Meigjers et al. (2014) proposed one numerical model "DCYCLE" to investigate the effects of the pre-shearing and random waves on the residual seabed response. Recently, Jeng and Zhao (2015) proposed a new definition of the source term and established a two-dimensional (2D) numerical model to consider the time-phased shear stress of seabed. The pore pressure distribution with both propagating and standing wave loading was investigated in their study. All the above investigations didn't consider the presence of the marine structure.

The static loading of a marine structure due to its self-weight increases the initial effective stress of soil, and then significantly affecting the residual response of seabed, particularly for a heavy marine infrastructures (Jeng et al., 2013; Ye et al., 2015). Based on an experimental study, Sumer et al. (1999; 2006) investigated the build-up of the pore pressure and corresponding liquefaction around a pipeline. Their studies indicated that liquefaction firstly occurred at the bottom of the pipe, and then developed upwards to the top-soil along the pile surface. Recently, Ye et al. (2015) developed an integrated numerical model for the residual response of seabed, which combines the Reynolds Average Navier–Stokes (RANS) wave model and an elastoplastic seabed model. The integrated model was applied to investigate the residual response of the sloping seabed around a composed breakwater. Zhao and Jeng (2016) investigated the pore pressure accumulation around the trenched pipeline in a half-buried seabed. They indicated that liquefaction might occur in the underlying trench layer if the backfill of the soil is shallow. The above investigations focused on the residual response of the seabed around breakwaters and buried pipelines, which are particularly limited to a 2D case without wave diffractions around the marine structure. For more discussions on the seabed response and liquefaction phenomenon around marine structures, readers can refer to de Groot et al. (2006a; 2006b).

The phenomenon of wave–seabed–mono-pile interaction is a typical 3D flow problem, in which the embedded depth of the pile and the wave reflection and diffraction significantly affect the residual response of seabed. Qi and Gao (2014) experimentally investigated the seabed response and scour around a mono-pile foundation in the lab, in which the pore pressures were measured by the pressure sensor buried in the seabed. Recently, several literatures are published for seabed instantaneous response around mono-pile and group pile foundations which are with QS (Quasi-static model) or PD (Partial dynamic) models (Duan and Jeng, 2018; Duan et al., 2018; Lin et al., 2017; Tong et al., 2018; Zhang et al., 2017). Sui et al. (2017) and Zhang et al. (2016) developed a more advanced fully dynamic (FD) seabed model to consider the inertial terms of soil skeleton and pore water. The range of application of the QS, PD, and FD models for the seabed oscillatory response can be found in studies by Ulker and Rahman (2009).

The aforementioned investigations focused on the oscillatory mechanism of soil response for mostly the sandy seabed with high permeability. Li et al. (2011) developed a finite element model for the seabed residual response around an embedded pile foundation. They showed that the seabed liquefaction is more serious at the rear of a pile. However, in their study, the wave reflection and diffraction were neglected, because they only focus on a pile with small diameter. More recently, Zhao et al. (2017a) numerically investigated the seabed residual response around a single pile by integrating a RANS wave model and a quasi-static soil model (QS model). Therefore, the inertial terms of soil skeleton and pore water were neglected in their study. However, the inertial terms of both soil skeleton or/and pore pressure (considered in the PD and FD model) can significantly affect the seabed response, particularly for the cases around marine structures (Jeng and Cha, 2003; Ulker et al., 2010). To the best of the authors' knowledge, the effect of the above-mentioned inertial terms on the residual response of seabed has not been investigated. Despite this, such important effect of wave transformation and the embedded depth of a pile on the residual response, was not systematically discussed in Zhao et al. (2017a).

In this study, a 3D numerical model WINBED (version 2.0) for the wave-induced residual response of seabed around a mono-pile foundation is developed. It should be noted that the previous version of the model (WINBED 1.0) of Sui et al. (2017) and Zhang et al. (2016) only deals with the oscillatory seabed response. The main contributions of the present WINBED 2.0 model are: (1) the residual response module of seabed has been added by using a 3D pore pressure source term (see Eqs. 9-16); and (2) the present model (WINBED 2.0) may be the first one that considers the acceleration of pore fluid and soil skeleton (inertial terms) in simulating the residual response of seabed.

The present paper is organized as follows: the governing equations, boundary conditions, numerical scheme, and operational process of the present model are presented in Section 2. Model validations based on five sets of flume tests available in the literature are illustrated in Section 3. Based on the model application, the wave-induced 3D distributions of the accumulated pore pressure and corresponding liquefaction around a mono-pile are discussed in Section 4. Through these discussions, the residual pore pressures owing to different simulation modes of the QS, PD, and FD formulations (effects of the inertial terms) are examined. The effects of wave reflection and diffraction on the residual response of seabed are analysed. The significance of the above effects with different vertical locations, wave steepness, soil permeability, and relative soil densities are studied. Seabed liquefaction around a mono-pile foundation is also investigated. Finally, several concluding remarks are given in Section 5.

2. Numerical Model

2.1 Seabed model

Following the previous study (Jeng, 2013), the wave-induced pore pressure (p) can be divided into two parts, namely the oscillatory (instantaneous) pore pressure (p_{ins}) and residual (accumulation) pore pressure (p_r) (see Fig. 1), which is expressed as

$$p = p_{ins} + p_r \tag{1}$$

The oscillatory pore pressure usually behaves cyclically in magnitude induced by each wave loading, and could be found with phase lag as well as the damping of amplitude in the vertical direction (Yamamoto et al., 1978). On the other hand, the residual pore pressure shows a progressive nature with time lasting. This is due to the volumetric contraction caused by the cyclic shear stress of soil (Seed and Rahman, 1978). In the following parts of section 2, both mechanisms for the wave-induced seabed response will be described in detail.

2.1.1 Oscillatory Mechanism

In this study, the Biot's poro-elastic theory is used to investigate the oscillatory response of seabed. The basic assumptions of the model are: (1) the soil skeleton and pore fluid are compressible; (2) the flow in the porous bed obeys Darcy's law; (3) the deformation of the porous seabed obeys the Hooke's law and (4) the effect of gas diffusing through water and movement of water vapour is ignored. It should be noted that the tensile stress may occur in the simulation as there is no "yield" criteria in the elastic model. However, the elastic model is popularly used due to its simplicity and numerous successful validation cases in engineering practice (Alcérreca-Huerta and Oumeraci, 2016; Jeng et al., 2013; Meijers and Luger, 2012). The governing equations in FD approximations can be written as follows (Zienkiewicz et al., 1980):

$$\sigma_{ij,j} + \rho g_i = \rho \ddot{u}_i + \rho_f \ddot{w}_i \tag{2}$$

$$-p_{ins,j} + \rho_f g_i = \rho_f \ddot{u}_i + \frac{\rho_f \ddot{w}_i}{n} + \frac{\rho_f g_i}{k_i} \dot{w}_i \tag{3}$$

$$\dot{u}_{i,i} + \dot{w}_{i,i} = -n\beta \dot{p}_{ins} \tag{4}$$

where σ_{ij} is the total stress, ρ is the average density of the porous medium, ρ_f is the density of pore water, g_i is the gravitational acceleration in the i-direction, u_i is the displacement of the soil matrix in the i-direction, w_i is the average relative displacement of the fluid to the solid skeleton in the i-direction, k_i is the permeability of the porous medium in the i-direction, n is the porosity of the solid phase.

The equivalent compressibility of pore water and entrapped air β is defined as (Verruijt, 1969):

$$\beta = \frac{1}{k_w} + \frac{1 - S_r}{\rho_f g d} \tag{5}$$

where d is the water depth, S_r is the saturation degree, k_w is the bulk modulus of the pure water which is taken as 1.95×10^9 N/m^2 (Yamamoto et al., 1978). This expression takes the saturation degree (S_r) into account for the deformation of porous medium. It is noted that this definition is only valid for a high saturation degree (e.g. $S_r \geq 0.95$) (Pietruszczak and Pande, 1996).

The total stress (σ_{ij}) can be expressed in terms of the effective stress (σ'_{ij}) and pore pressure (p), and the effective stress-strain relation can be written as:

$$\sigma_{ij} = \sigma'_{ij} - \delta_{ij} p_{ins} \tag{6}$$

$$\sigma'_{ij} = \lambda \varepsilon_{kk} \delta_{ij} + 2G\varepsilon_{ij} \tag{7}$$

$$\varepsilon_{ij} = \frac{u_{i,j} + u_{j,i}}{2} \tag{8}$$

where δ_{ij} is the Kronecker delta denotation, σ'_{ij} is the effective stress, ε_{ij} is the soil strain, λ=2$G\mu$(1-2μ), G is the shear modulus, μ is Poisson's radio. Note that the above definition implies a positive tensional stress.

2.1.2 Residual Mechanism

Following the previous investigations of Seed and Rahman (1978), Sumer et al. (2012) for 1D case and Jeng and Zhao (2015) for 2D case, the numerical simulation of wave-induced residual response of the seabed around a marine structure is conducted in 3D space by this study. The governing equation for the pore pressure accumulation in the present model is:

$$\frac{\partial p_r}{\partial t} = c_{v3}\left(\frac{\partial^2 p_r}{\partial x^2} + \frac{\partial^2 p_r}{\partial y^2} + \frac{\partial^2 p_r}{\partial z^2}\right) + f_3(x,y,z,t) \tag{9}$$

where c_{v3} is the coefficient of the soil consolidation and $f_3(x,y,z,t)$ is the source term of the pore pressure generation in 3D space, which can be defined as:

$$C_{v3} = \frac{kE}{3(1-2\mu)\gamma_w} \tag{10}$$

$$f_3(x,y,z,t) = \frac{\sigma'_{03}}{T}\left[\frac{|\tau_{ins3}(x,y,z,t)|}{\alpha_r \sigma'_{03}}\right]^{-\frac{1}{\beta_r}} \tag{11}$$

where E is the Young's modulus of soil, γ_w is the unit weight of pore fluid, T is the period of wave loading; α_r and β_r are the empirical parameters which are defined from the following expressions (Sumer et al., 2012):

$$\alpha_r = 0.34 D_r + 0.08 \tag{12}$$

$$\beta_r = 0.37 D_r - 0.46 \tag{13}$$

$$D_r = \frac{e_{\max} - e}{e_{\max} - e_{\min}} \tag{14}$$

where D_r is the relative density of soil.

In Eq. (11), σ'_{03} is the initial soil effective stress at the final state of seabed consolidation, $\tau_{ins3}(x,y,z,t)$ is the phase-resolved shear stress obtained from the oscillatory model (see Section 2.1.1), which are expressed as:

$$\sigma'_{03} = \frac{1}{3}(\sigma'_{x0} + \sigma'_{y0} + \sigma'_{z0}) \tag{15}$$

$$\tau_3(x,y,z,t) = \sqrt{\tau_{xz}^2(x,y,z,t) + \tau_{yz}^2(x,y,z,t) + \tau_{xy}^2(x,y,z,t)} \tag{16}$$

It should be noted that the shear stress of soil (τ) is defined as the maximum $\tau_{(max)}$ within one wave period by Seed and Rahman (1978) in their 1-D model, and is defined as the instantaneous τ_{xy} by Jeng and Zhao (2015) in their 2-D model. Li and Jeng (2008) further set it as $\tau_3 = (\tau_{xy} + \tau_{yz} + \tau_{xz})/3$ based on an averaged concept, and applied it for the 3D seabed residual response around a breakwater head. However, the above definition of Li and Jeng (2008) may significantly underestimate the amplitude of pore pressure (Fig. 6). In this study, the shear stress is defined (Eq. 16) based on the resultant force concept in 3D space. The comparison between the previous (Li and Jeng, 2008) and present (Eq. 16) definition in simulating the residual response of seabed is presented in chapter 3.

2.2 Wave model

The "FUNWAVE 2.0" open-source code is adopted to calculate the wave pressures at the soil-water interface and soil-structure interface, which are used as the input in the seabed model. "FUNWAVE" code was first developed at University of Delaware (Kirby et al., 2003) based on the nonlinear Boussinesq equations of Wei et al. (1995), and is now commonly used in simulating wave motion in the coastal area. Consequently, Shi et al. (2001) further discretized the equations on the staggered grid in the generalized curvilinear coordinates in order to better fit the complex configuration boundary. In FUNWAVE, different levels of Boussinesq approximations can be chosen by setting an equation ID in the input file. The main advantage of FUNWAVE is to simulate the wave transformations around marine structures for a relatively large coastal area (comparing to the CFD model (Zhang et al., 2014)). However, the limitation is that it is hard to deal with the complex wave breaking in front of a structure. The FUNWAVE model has also been successfully adopted in the previous study of Sui et al. (2016) for the oscillatory response of seabed. For more detailed information regarding the governing equations as well as the numerical techniques, readers can refer to Kirby et al. (2003).

2.3 Boundary Conditions

To solve the governing equations, appropriate boundary conditions are required. Fig. 2 shows a 3D sketch of the boundary conditions used in the present model. The seabed is assumed to be impermeable and rigid at the lateral and bottom boundaries. Therefore, the seabed displacements and the normal gradients of both oscillatory and residual pore pressures are zero:

$$u_{soil} = 0, \quad \frac{\partial p_{ins}(p_r)}{\partial n} = 0 \tag{17}$$

At the seabed surface, effective normal stress vanish. The shear stress is also neglected as it is minor comparing to the maximum dynamic pore pressure in this study (Ye and Jeng, 2011; Liang et al., 2008; Zhang et al., 2015). The wave-induced oscillatory pore pressure is equal to dynamic wave pressure, and the residual pore pressure is zero without any contraction of soil skeleton:

$$p_{ins} = p_w, \quad p_r = 0, \quad \sigma'_{soil} = 0, \quad \tau_{soil} = 0 \tag{18}$$

At the structure-seabed interface, the normal gradient of pore pressures is zero, while the seabed displacement is equal to that of structure. This "no-slip" boundary is usually assumed in the previous studies, which is reasonable due to the minor displacements of marine structures (Mizutani et al., 1998).

$$\frac{\partial p_{ins}(p_r)}{\partial n}, \quad u_{soil} = u_{pile}, \quad \sigma'_{pile} = \sigma'_{soil} - p, \quad \tau_{pile} = \tau_{soil} \tag{19}$$

At the water-structure interface, the structure normal stress is equal to the wave pressure, the shear stress is assumed to be zero. Note that, this indicates a one-way coupling between water and structure.

$$\tau_{soil} = 0, \quad \sigma'_{pile} = p_w \tag{20}$$

At the air-structure interface, all stresses are set to zero by assuming that the effects of the wind/aerodynamic is minor to be neglected:

$$\tau_{soil} = 0, \quad \sigma'_{pile} = 0 \tag{21}$$

2.4 Integrating procedure

The present “WINBED” model consists of two seabed modes, which are the oscillatory mode and residual mode. Note that, two-way coupling for structure-soil (Eq. 19) while one-way coupling (Eq. 20) for wave-structure are applied in this model. At the beginning of the simulation, model initialization and grid generation are conducted, and the boundary conditions are assigned according to Eqs. (17-21). At one time-step, the oscillatory mode is first solved to obtain the seabed oscillatory variables (u_x, u_y, u_z, w_x, w_y, w_z, p_{ins}). The soil effective stress is then obtained based on the strain-stress relation of soil, and these are the input for the residual mode. The simulation results show that the relative error of residual pore pressure significantly decreases with the increase of the iteration steps. In this study, the threshold relative error between two successive iteration steps is set as 0.0001 (usually realized after about 100 iteration steps). Computation will be terminated when this simulation accuracy is achieved.

3. Model validation

Five cases are conducted against the previous experimental data to validate the present model. Case 1 (Fig. 4) is for the water wave elevation around a mono-pile foundation (Cong et al 2015). Case 2 (Fig. 5) is for the oscillatory seabed response under pure wave loading (Lu 2005). Cases 3 (Fig. 6) and 4 (Fig. 7) are for the residual seabed response under pure wave loading (Sumer et al. 2012; Kirca et al. 2013). Case 5 (Fig. 8) is for the wave-induced seabed response around a mono-pile foundation, where the oscillatory response dominates in the experiment (Qi and Gao 2014).

Cong et al. (2015) conducted a series of physical experiments to measure the water wave surface elevations around 2 × 2 group of circular piles. The experiments were carried out in a wave basin to measure the wave reflection and diffraction caused by the wave–pile interaction. The parameters used in the experiments for this validation include the water depth of d = 0.5 m and the pile diameter of D = 0.4 m. Fig. 4 shows a comparison of the water surface elevation at three orientations corresponding to α = 0, 22.5º, and 45º with respect to the wave incident direction. Wave period T and wave amplitude A are shown in Fig. 4. The wave surface elevations in G6 of α = 22.5º (Fig. 4b) show an irregular and relatively flat sinuous formation, whereas the wave elevations in G5 of α = 0º (Fig. 4a) and G3 of α = 45º (Fig. 4c) show an irregular fluctuation, which are due to the interaction of the wave with the pile. As shown in Fig. 4, the present model reproduces the experiment results well, indicating that the present model can simulate the non-linear wave transformation around piles with high accuracy.

For the second validation, the present model is compared with the flume test conducted by Lu (2005) on the seabed oscillatory response under linear/cnoidal wave loading. In the experiments, several pressure sensors were installed within soil at different depths of 0, -5, -10, and -15 cm from the soil surface. The parameters for the wave and seabed are: seabed depth, h = 20 cm; permeability, $k = 1.4\times10^{-3}$ m/s; Young's modulus, $E = 1.4 \times 10^{7}$ m/s; poison's ratio, μ = 0.33; and porosity, n = 0.39. The linear wave case use period, T = 1.2 s; depth, d = 0.5 m; and height, H = 0.12 m, whereas the cnoidal wave case uses period, T = 1.4 s; depth, d = 0.3 m; and height, H = 0.14 m. Fig. 5 shows a comparison of the simulated and measured dynamic pore pressures under the linear wave (figures in the left-side column) and cnoidal wave (figures in the right-side column). As Fig. 5 indicates, the fluctuation of pore pressure under a cnoidal wave is sharper and thinner than that under a linear wave, whereas the amplitude of the pore pressure with a cnoidal wave is much larger. Fig. 5 also reveals that the dynamic pore pressure decreases with an increase in distance from the soil surface, which is because the pore water velocity dramatically decreases when going deep into the seabed.

Fig. 6 shows a comparison of the simulated (Li and Jeng, 2008; Sumer et al., 2012; and the present study) and measured (Sumer et al., 2012) pore pressure accumulations (residual response) within a silt seabed under progressive wave loading. The parameters for the wave and seabed are: seabed depth, h = 40 cm; permeability, $k = 1.0 \times 10^{-5}$ m/s; Shear modulus, $G = 1.92 \times 10^{6}$ m/s; Poison's ratio, μ = 0.29; porosity, n = 0.51; submerged specific weight of the soil, γ' = 8.14 kN/m^3; degree of saturation, S_r = 1; wave period, T = 1.6 s; wave height, H = 0.18 m; and water depth, d = 0.55 m. It should be noted that, the pressure oscillations recorded in the physical model are mainly caused by the oscillatory seabed response (Sumer, 2014). To better demonstrate the residual pore pressure, the oscillatory part has been manually removed, following the previous studies of Sumer et al. (2012), Kirca et al. (2013) and Jeng and Zhao (2015), depicted in Fig. 7. As is shown in Figs. 6a and 6b, the averaged shear stress ($\tau_{average} = 1(|\tau_{xy}|+|\tau_{xz}|+|\tau_{yz}|)/3$) by Li and Jeng (2008) may significantly underestimates the measured accumulated pore pressure, whereas the definition in eq. (16) shows an overall agreement. The numerical results adopting the maximum 3D shear stress (τ_{3max}) of this study (Eq. 16), are very close to those of Sumer et al. (2012). An overall trend of the residual pore pressure in the present study agrees well with the experiment data. It is noted that the maximum pressure ratio p/σ'_{v0} is 0.98; indicating that the seabed is between the partial liquefaction (p_r/σ'_{v0} = 50%) and full liquefaction (100%) (close to the full liquefaction). This validation also demonstrates that the present model improves the numerical accuracy of the 3D residual response over that found by Li and Jeng (2008).

The fourth validation case is the experiment by Kirca et al. (2013) who studied the residual liquefaction under a standing wave in a detailed systematic manner in a physical model investigation. Fig. 7 shows the comparison of a simulated and measured (Kirca et al., 2013) pore pressure build-up within the silt seabed under a standing wave. The soil conditions for the experiments were the same as in the third validation (Sumer et al., 2012). The wave parameters for the current case are: wave height, H=10.2 cm; wave period, T=1.09 s; water depth, d=0.3 m. It should be noted that, a sealed plate was used to separate the silt seabed; This is different from the configuration utilized in simulation domain, and this slightly affects the simulation results. Overall, the numerical results capture the trend of the accumulated pore pressure as shown in Fig. 7, and this validates the capability of the present model in dealing with the accumulated pore pressure under a standing wave.

The final validation case involves a mono-pile foundation. The experiment of Qi and Gao (2014) is selected. Qi and Gao (2014) carried out a series of flume tests to investigate the wave/current-induced seabed instability (scouring and liquefaction) around a pile. In the present study, the measured data with only wave loading prior to scour are used to validate the present model. The parameters of the wave, seabed, and mono-pile are: seabed depth, h = 0.5 m; permeability, $k = 1.0 \times 10^{-3}$ m/s; Young's modulus, $E = 3.84 \times 10^7$ m/s; Poison's ratio, $\mu = 0.33$; porosity, $n = 0.435$; wave period, $T = 1.0$ s; height, $H = 0.08$ m; depth, $d = 0.5$ m; pile radius, $R = 0.2$ m; and pile embedded depth, $l_p = 0.3$ m. Fig. 8 shows a comparison of the simulated and measured vertical pore pressure distribution in front of and behind the pile. As illustrated in Fig. 8, the pore pressure in front of the mono-pile is greater than behind, but decreases more rapidly. This is because the wave loading increases in front of the pile owing to the wave reflection and diffraction. In general, the simulated pore pressure around the mono-pile agrees well with the measurements.

4. Model applications

In this section, the present model is applied to investigate the wave-induced seabed residual response around a mono-pile. Model sketch for the parametric study is shown in Fig. 2. There are two application cases in this study. The first application (Figs. 9-19) is to investigate the effect of wave diffraction/reflection on the residual response around mono-pile. The second application (Figs. 20-25) is to investigate the effect of the pile embedded depth on the residual response and liquefaction of its surrounding seabed. For the first application, the pile parameters (R_p, E_p, μ_p, l, d_e), water depth (d), water density (ρ_f), seabed porosity (n), submerged weight (γ_s) are fixed. For the second application, only the parameter of pile inserted depth is varied. To investigate a relatively obvious wave diffraction/reflection phenomenon, the wave steepness for the first application are relatively small, which corresponds to a weak residual response. Parameters of the wave, the seabed and the mono-pile for the first application are listed in Table 1; while parameters for the second application are listed in Table 2.

4.1 Consolidation state

In natural environments, the seabed will be subjected to a long-time consolidation under the weight of static water and the seabed itself. The basic assumption of this study is that the seabed can be further compressed by the wave loading after the long-time consolidation process under the static water and pile gravity. The assumption is reasonable especially with large wave loading, as soil particles can become more adjacent between each other due to the back-and-forth movement caused by the cyclic shear stress. This assumption is commonly adopted in many previous studies (e.g. Seed and Rahman, 1978; Sumer 2014). In this situation, the final consolidation state is important as it implies the initial resistance to liquefaction prior to wave loading (Sui et al., 2017; Ye et al., 2015; Li et al., 2017).

Fig. 9 illustrates the final consolidation state of the seabed for (a) pore pressure, (b) effective stress and (c) subsidence in the vicinity of a mono-pile. After the long-time consolidation, the pore pressure (p) was found layered in the vertical direction (Fig. 9a). Fig. 9b shows the spatial distribution of effective stress (σ'_z) around the mono-pile. It was seen that the effective stress below the pile is remarkably increased, which is due to pile gravity being completely supported by the soil skeleton after a long-time consolidation. In addition, the phenomenon of stress concentration was found at the corners of the pile. This is probably caused by the sharp change of Young's modulus between the seabed and pile. As a result, the seabed below the pile suffers the largest subsidence (Fig. 9c) because of the large soil effective stress there.

4.2 Wave transformation

Fig. 10 shows the water surface elevations with wave reflection and diffraction around the mono-pile. It was found that the presence of the mono-pile increases and decreases the wave height in front of and behind the mono-pile, respectively. Specifically, when the wave trough arrives at the head of the pile (t = 2.95 T), the largest negative wave pressure will be generated at the bottom of the water. For t = 3.45 T, the wave crest arrives at the same location, generating positive pressure. Owing to the wave reflection and diffraction, it was found (Fig. 10) that a specific zone in the front and rear sides (dashed line in Fig. 10a) relative to the pile has the largest variation in wave height (H). This phenomenon can significantly affect the spatial features of the accumulated pore pressure (see Fig. 11 in section 4.3). It should be noted that the wave reflection and diffraction provide a 3D wave loading at the interfaces of water-seabed and water-structure.

4.3 Cyclic stresses and pile displacements

Cyclic wave loading would cause cyclic stresses and cyclic pile displacements, and they come from the oscillatory part of the model in this study. Fig 11 illustrates the distributions of pore pressure p_{ins} (coming from the oscillatory part of pore pressures

(Eq. 1)), effective stress σ'_x and σ'_z, and shear stress τ_{xz} around the mono-pile foundation Fig. 11 show that the positive pore pressure and negative effective normal stresses (σ'_x and σ'_z) are found under the wave crest. Relatively large shear stresses τ_{xz} is found between the wave trough and wave crest. It is seen that at t=0.5T, relatively large positive shear stress is found at the head of the pile foundation, which would cause a relatively large power (large source term f) to generate the residual pore pressure. As a result, the cyclic motion of pile is found, as shown in Fig. 12. Horizontal displacement of pile behaves cyclically under the dynamic wave loading. It should also be noted that, different from most of the previous studies that set a fixed mono-pile, the pile displacements at the bottom are not zero (see Fig. 12). This is because pile movement is allowed in this study by applying the two-way coupling of soil-pile interaction.

4.4 Pore pressure accumulation

In above application cases, only the residual pore pressure is considered as the seabed has poor drainage. Numerical simulation shows that the amplitude of the oscillation in pore pressure is much smaller than the residual pore pressure in the application cases. Therefore, the peak value caused by the oscillatory pore pressure may not significantly affect the onset of liquefaction in this study.

Fig. 13 illustrates the 3D temporal and spatial features of the accumulated pore pressure (p_r) around the mono-pile for (a) t = 35 s in the x-z section (y/R_p=0), (b) t = 35 s in the x-y section (z/R_p=-0.75), (c) t = 600 s in the x-z section (y/R_p=0), and (d) t = 600 s in the x-y section (z/R_p = -0.75). At t = 35 s, the pore pressure is relatively small (Fig.

13a), then it increases gradually with time (Fig. 13c). A similar trend of the pore pressure build-up in the *x-y* section can be seen in Figs. 13b and 13d. In addition, Figs. 13b and 13d indicate that the largest pore pressure (p_r) appears at the locations near the front (π/4 with respect to the incident wave direction) and rear (3π/4) sides of the pile. This distribution pattern is due to the significant change in wave surface elevations occurring there (see the dashed line in Fig. 10). A significant change in wave loading (owing to the wave height) will increase the shear stress (τ_{xz}, τ_{yz}, and τ_{xy}) of the soil skeleton. This would lead to a large source term (f) which generates a large pore pressure there.

Fig. 14 shows the effects of wave period (T) on the residual pore pressure p_r (in the *x-y* plane) in the vicinity of the mono-pile foundation (after 150 wave cycles). The concerned points have been selected along a half-circle with $S/R_p = 1$ and $z/R_p = -1$ (where S is the distance from the mono-pile surface). The angle α denotes the relative position with respect to the mono-pile, which varies from zero (at the front of the mono-pile) to π (at the rear of the mono-pile). Three dashed lines are plotted in Fig. 14 indicating the iso-pressure (p_r = 60, 120, and 180 Pa) of the pore fluid. It was found that an increase in wave period greatly increases the amplitude of residual pore pressures within the vicinity of the mono-pile. That is, due to large wave periods generating a large wave loading at the seabed surface, thereby promoting compression of the soil particles. In addition, the residual pore pressure is found to increase and decrease in front of and behind the mono-pile, respectively, which is due to the wave transformation. The shape of the pore pressure distribution becomes more symmetric with respect to the pile centre when the wave period T increases (from 4 to 8 s). It is noted that the above effects may be only important in relatively shallow water, as the phenomenon of wave diffraction and reflection is usually more pronounced in shallow water.

Fig. 15 illustrates the effects of the permeability k, degree of saturation S_r, Young's modulus E_s, relative density D_r, residual coefficient (α_r and β_r) on the residual pore pressure around the mono-pile. The vertical distribution of the residual pore pressures in front of the pile (x/R_p = -3.5 and y/R_p = 0) is plotted at t = 600 s (150 wave cycles). The relatively low seabed permeability k results in poor drainage conditions, which hinders the pore pressure dissipation in the seabed. This further leads to a relatively high residual pore pressure (Fig. 15a). The decrease in the degree of saturation corresponds to the increase of the residual pore pressure (Fig. 15b). This is because the decrease of saturation leads to an increase in the seabed shear stress (τ_{xz}), which in turn strengthens the compression of the soil. It is noted that the difference of pore pressure between cases having S_r=0.992 and S_r=0.985 is much smaller than between S_r=0.985 and S_r=0.98. This indicates that in a nearly saturated seabed (e.g. S_r>0.985), the residual pore pressure does not change much with the increase in S_r. Fig. 15c and Fig. 15d shows the effects of Young's modulus (E_s) and relative density (D_r) on the residual pore pressure around the mono-pile. It illustrates that, the increase of E_s and D_r would cause the decrease of the amplitude of residual pore pressure. This is because the relative large Young's modulus (E_s) and soil relative density (D_r) corresponds to a relatively "dense" seabed; which would be more difficult to be compressed by the wave loading. Fig. 15e and Fig. 15f examine the effects of the coefficients α_r and β_r, respectively. It is found that the residual pore pressure increases with the decrease of α_r and β_r. This is in accordance with the change in eq. (11) for the pressure source term. The decrease of α_r and β_r would cause an increase of the source term (f_3) (negative correction), leading to an increase of the pore pressure. This is obtained providing that the $\tau_{ins3}/(\alpha_r\sigma'_{03})$ of Eq. 11 is less than 1. We can deserve it would have a positive correction between β_r and source term (f_3) if $\tau_{ins3}/(\alpha_r\sigma'_{03})$ is greater than 1.

4.5 Effects of inertial terms on the accumulated pore pressure

Three different numerical models, namely the FD, PD, and QS models, for seabed oscillatory mechanism were proposed to investigate the effects of the inertial terms of the soil skeleton/fluid (Zienkiewicz et al., 1980). The governing equations for the FD model are shown in eqs. (2)–(4). Ignoring the accelerations from the pore fluid and/or soil motion simplifies these general formulations into a conventional PD or QS model.

Fig. 16 illustrates the vertical distribution of the residual pore pressure with FD, PD, and QS models. Here, Δp_{r1} denotes the discrepancy in the residual pore pressure between the QS and PD models, and Δp_{r2} denotes this discrepancy between the PD and FD models. The selected section is directly in front of the pile (x/R_p=-1.53, y/R_p=0). Fig. 16 shows that almost no discrepancy (Δp_{r2}) is found between the PD and FD models. This is because the inertial terms effects of pore fluid on the seabed shear stresses is minor for the case with wave loading (Ulker and Rahman, 2009), which leads to a small discrepancy in residual pore pressure. As the comparison shows, the simulated residual pore pressure using the QS model is smaller than that using the FD or PD model. This indicates that the seabed residual response will be underestimated if the inertial terms of the pore fluid and soil skeleton are neglected.

Fig. 17 shows the vertical distributions of the relative difference of pore pressure (Δp_{r1}/max(p_{QS})) in front of (point A), at the side (point B), and at the rear (point C) of the mono-pile. Note that, the max(p_{QS}) indicates the maximum pore pressure with QS model. It is found that the relative difference (Δp_{r1}/max(p_{QS})) first increases with the increase in the seabed depth at the top layer (i.e. $-0.8<z/R_p<0$), and then decreases as the seabed deepens ($z/R_p<-0.8$). This indicates that the largest effect of the inertial terms on residual pore pressure is found at the middle part of the seabed ($z/R_p=-0.8$ in this study). In addition, the relative difference Δp_{r1}/max(p_{QS}) is found to be the largest in front of the mono-pile (point A) comparing to that at point B (at the side) and point C (at the rear). This indicates that the effect of the inertial term is largest in front of pile. This is because the wave loading in front of pile is larger due to wave reflection and refraction. It should be noted that, the largest relative difference (Δp_{r1}/max(p_{QS})) can reach 3.8% and Δp_{r2}/max(p_{QS})$\approx$0 (depicted in Fig. 16). This indicates that the PD model should better be used and is sufficient in simulation of wave-induced residual response. This conclusion is in accordance with Ulker and Rahman (2009) which is for the oscillatory response, and is extended to the residual response of seabed by the present study. However, it should be noted that, the effect of the inertial terms is overall small (the maximum difference is 3.8% p_0 in this study); which could be neglected in the engineering practice.

4.6 Significance of the mono-pile foundation for the accumulated pore pressure

Fig. 18 shows a comparison of the accumulated pore pressure with and without a mono-pile foundation. The concern point is in front of the pile with coordinates of $x/R_p = -3.5$, $y/R_p = 0$, and $z/R_p = -0.83$. As shown in Fig. 18, the increase in accumulated pore pressure is relatively faster at the early stage of the wave loading ($t<200$ s). This then gradually decelerates until the residual pore pressure reaches a relative steady state ($t = 600$ s). Fig. 18 also shows that the time for the residual pore pressure to reach a relatively steady value is approximately the same ($t = 600$ s) for the cases with and without the mono-pile. This indicates that such a build-up pattern of pore pressure is independent of the magnitude of the wave loading at seabed surface.

The discrepancy in the maximum pressure value (Δp_r) between the two cases (with and without a mono-pile) is defined as the significance of the mono-pile on the residual response of seabed. Fig. 19 illustrates Δp_r with various vertical locations (z), wave steepness (H/L), permeability (k), and relative seabed densities (D_r). It was found that this significance (Δp_r) increases with an increase in depth at the upper part of the seabed ($-0.83 < z/R_p < 0$), and then decreases when the seabed deepens ($z/R_p < -0.83$) (Fig. 19a). Figs. 19b–19d illustrate the change in Δp_r with various wave and seabed parameters ($x/R_p = -3.5$, $y/R_p = 0$, and $z/R_p = -0.83$). It was found that the significance of a mono-pile for the residual response of seabed increases with the increase in wave steepness (H/L) (Fig. 19b), and decreases with the seabed permeability (k) (Fig. 19c) and relative seabed density (D_r) (Fig. 19d). This is due to the fact that the increase in wave steepness (H/L) will increase the magnitude of the residual pore pressure. Increases in seabed permeability (k) and relative seabed density (D_r) will decrease the residual pore pressure because they improve the soil drainage conditions (for k) and restrain the compression of soil particles (for D_r).

4.7 Residual liquefaction

Zen and Yamazaki (1990) proposed the following 1D liquefaction criterion:

$$-(\gamma_s-\gamma_w)z \le p_0 - p_{b0} \tag{22}$$

where p_0 is the wave-induced pore pressure, p_{b0} is the dynamic wave pressure at the seabed surface, and γ_s and γ_w are the specific bulk weight of the soil (not the grains) and water, respectively.

Jeng (1997) extended this criterion to a 3D situation by adopting the concept of average effective stress, namely,

$$-(\gamma_s-\gamma_w)\frac{1+2k_0}{3}z \le p_0 - p_{b0} \tag{23}$$

where k_0 is the lateral compression coefficient of the soil.

The above criteria are only suitable for the cases without a marine structure. When a structure is present, the soil skeleton in the vicinity of the structure will be compressed, which suppresses the occurrence of soil liquefaction (Jeng, 1997). In addition, Eqs. (22) and (23) provide the criteria for an instantaneous liquefaction (Sumer, 2014), which is likely to occur in a sandy seabed. For a silt seabed, the residual mechanism dominates the seabed response. Therefore, liquefaction is mainly due to the excess residual pore pressure (p_r - 0) caused by the compression of soil skeleton (Liao et al., 2015). Following previous studies (Ye, 2012; Liao et al., 2015), the residual liquefaction criterion that considers the weight of mono-pile can be expressed as follows:

$$\sigma'_{z0} \le p_r \tag{24}$$

where σ'_{z0} is the initial normal effective stress obtained from the final state of consolidation (see section 4.1). The dynamic Biot equation is adopted in this study, based on the assumption that seabed is seen as a porous elastic media (Sumer, 2014). It has to be clarified that the present work only predicts the potential liquefaction depth rather than simulating the real liquefaction process. In this section, the present model is adopted to investigate the wave-induced residual liquefaction potential around a mono-pile, taking into consideration the state of the seabed consolidation. The parameters utilized in this simulation are listed in Table 2.

Fig. 20 illustrates the residual pore pressure (p_r) and liquefaction depth (l_d) around the mono-pile at t = 40 s (a, c, and e) and t = 792 s (b, d, and f). Initially (t = 40 s), a relatively large residual pore pressure mainly appears within the vicinity of the mono-pile ($-5<x/R_p<5$, $-3< y/R_p <3$, zone A), whereas the location far from the pile ($|x/R_p|>5$, $|y/R_p|>3$, zone B) have a relatively small pore pressure (Fig. 20a). As a result, Figs. 20c and 20e illustrate that liquefaction only occurs close to the mono-pile foundation (zone A). Comparing with Fig. 18a, the pore pressure at t = 792 s is largely increased especially away from the pile (zone B) (Fig. 20b). Correspondingly, the liquefaction depth (l_d) significantly increases in zone B (l_d/R_p increases from 0 to 1.2 m) (Figs. 20d and 20f). It was also found that the largest liquefaction depth (l_d) appears at the rear of the pile instead of at the front, which is consistent with the main findings of Li et al. (2011). Fig. 20f also shows that the liquefaction zone affected by the presence of the mono-pile (shown as the red dashed line) is approximately three-times the pile diameters (one pile diameter in front and two times the diameter in the rear) in length along the wave propagation direction (x-direction), and one pile diameter in width at the sides of the pile (y-direction). This demonstrates that the seabed in this area is prone to be liquefied, which therefore requires a special concern in engineering practice.

Fig. 21 illustrates the liquefaction depth (l_d) around the mono-pile with various embedded depths of the pile (de/R_p). The case without a pile foundation is also included for comparison. It was found from Fig. 21a that, for the case without the mono-pile, the liquefaction depth remains as z/R_p=-1.2 in the x-direction, which is consistent with the main conclusion of Jeng and Zhao (2015) that a 1D pattern of the liquefaction depth exists at the final state. The previous studies mostly investigate the seabed response around composite breakwater (de = 0) (Zhao et al., 2017b), and this study further reveals the liquefaction depth when a structure (e.g. a mono-pile) is embedded into the seabed (de > 0). It is found that, the liquefaction depth is small adjacent to the pile foundation due to the fact that the large resistance of soil skeleton exists there. In addition, the liquefaction depth (l_d) would decrease as the inserted depth of the pile is increased. This is mainly due to the decrease in the initial effective stress (σ'_{z0}) with increasing inserted depth (Sui et al., 2017), thereby leading to a significant decrease in soil overburden pressure.

The failure of seabed around the structure may also occur even with the a partially liquefied seabed. Such a partially liquefied seabed is usually referred to as Partial Fluidized Sediments (PFS) (Sumer, 2014; Zhang S. et al., 2018). The fluidization degree (f_d) (the ratio of excess pore pressure to the initial effective stress) is used to describe how much of sediment is fluidized, given by:

$$f_d = u/\sigma'_{v0} \qquad (25)$$

In which, u is the excess pore pressure and is equal to p_r in the present study.

Full liquefaction is seen as corresponding to 100% fluidization (f_d) as indicated in Equation (24) (Jeng, 2013; Kirca et al., 2013; Liao et al., 2018; Sumer, 2014; Zen and Yamazaki, 1990). As indicated above, full liquefaction is seen as the extreme state of the sediment fluidization (again, 100% fluidization) process, corresponding to the complete loss in resistance of the soil skeleton. This is a useful indicator to describe the most dangerous situation of the seabed. The relative cyclic shear stress ratio τ_c/σ'_{v0} (CSR, contributing to the source part f_3 in Eq. 11 plays an important role as it generates the excess pore pressure.

Fig. 22 shows the fluidization degree p/σ'_{v0} as well as the relative cyclic shear stress ratio (CSR) in front of and at the rear of the pile (see below). It is seen that the fluidization degree is zero at the seabed surface, and increases with time (Fig. 22a and Fig. 22b). Relatively large fluidization degree is found at the rear of the mono-pile. This indicates that liquefaction would easily happen there (u/σ'_{v0} exceeds 1). This is mainly because the cyclic shear stress ratio (CSR) is larger at the rear of the pile, which promotes more compression of the soil (Fig. 22c and Fig. 22d). The above conclusion is consistent with the previous study of Li et al. (2011) and Fig. 20 of the present study. Fig 22 a and b shows that the ratio u/σ'_{v0} is greater than 1 at the seabed surface, indicating that the soil particles have a potential trend to be separated (liquefaction already happens there) (Liu et al., 2015). This (u/σ'_{v0}>1) occurs because of the use of the elastic model, and cannot be rigorously avoided as there is no yielding criteria. In fact, the maximum liquefaction depth predicted with elastic model may be larger than that with a plastic model, due to the fact that the pore pressure is difficult to release with the elastic model (Qi and Gao, 2018). Such conservative approach benefits the foundation design in engineering practice.

Fig. 23 illustrates the effects of the relative density D_r on the liquefaction depth around mono-pile. It is found that the liquefaction depth decreases with the increase of the relative density D_r. This is because the relatively large D_r means a much more sand densification with a relatively low residual pore pressure generation. Noted that, there may be pre-shearing effects during the wave loading process (de Groot et al., 2006a; de Groot et al., 2006b; Meijers and Luge, 2012). The pre-shearing effect will increase the soil relative density (D_r) due to the sand densification. Therefore, Fig. 23c indicates that the pre-shearing effects can decrease the maximum liquefaction depth, which is in accordance with the main finding of Meijers and Luger (2012). This can provide the readers a basic understanding on the pre-shearing effects.

Fig. 24 illustrates the parametric studies for the effects of coefficients α_r and β_r on the liquefaction depth around mono-pile foundation. Fig. 24 shows that, the liquefaction depth decreases with the increase of α_r while it decreases with the decrease of β_r. This figure also shows, the liquefaction depth decreases with the increase of α_r while it decreases with the decrease of β_r. It is also found, effects of coefficient α_r on the liquefaction depth far away the pile is much larger than that near the pile. While for the coefficient β_r, the location at the vicinity of the pile owns the larger effects. With comparison, the effects of β_r on the liquefaction depth is obviously smaller than that of the α_r. Noted that, the scale effect may occur when the results are extended to the application in the real environment. The empirical formulas (Eq. 12 and Eq. 13) involving α_r and β_r, are obtained from a curve-fit exercise to the large-scale simple shear test data (De Alba, 1976; Sumer et al., 2012). It should be noted that, in this sense, the present simulations have already considered the scale effects based on the full-scale coefficients used.

Partial liquefaction is also often found in the real environment, which would cause a large decrease in soil effective stress and thus leading to the instability of the foundation. Partial liquefaction may happen if the fluidization degree $p_r/\sigma'z$ is greater than e.g. 0.5 (it is 1 for the full liquefaction, see Eq. 24) (de Groot et al., 2006a; de Groot et al., 2006b). Fig. 25 shows the comparison of liquefaction depth between the full liquefaction criteria and partial liquefaction criteria. It illustrates that the estimated liquefaction depth with partial liquefaction criteria is much larger than that with the full liquefaction. This indicates that the design strategy with a partial liquefaction criteria should be much safer in the practical offshore engineering. It is also found that, with the partial liquefaction criteria, the liquefaction depth near the pile does not change much comparing to that far away from the pile. This indicates that the effect of the presence of pile on the liquefaction depth is much weaker with the partial liquefaction criteria.

5. Conclusion

In this study, based on a non-linear Boussinesq wave model and FD seabed model, a 3D integrated numerical model was developed to investigate the wave-induced residual response of the seabed around a mono-pile foundation. Experimental data from five flume tests were used to validate the present model. Good agreement between the measured data and numerical simulations was obtained. The validated model was then applied to investigate the pore pressure accumulation around a mono-pile foundation. Considering the self-gravity of the pile, the wave-induced 3D liquefaction zone around an embedded pile foundation was investigated. The following conclusions were drawn:

(1) The present numerical model adopting the definition of the 3D source term f_3 can provide reliable results with regard to pore pressure accumulation around a marine structure.

(2) Wave diffraction and reflection increase and decrease the residual pore pressure in front and at the rear of a mono-pile, respectively. Effects of wave diffraction/reflection increase with an increase in wave height (H) and a decrease in wave period (T), seabed permeability (k), and relative density (D_r).

(3) The increase of the residual pore pressure is relatively faster during the early stage of wave loading, then gradually decelerates until the pore pressure reaches a relatively high value. Such the build-up pattern of pore pressure is independent of the magnitude of wave loading.

(4) This study presents a direct comparison among the FD, PD, and QS models. It is found that the wave-induced residual response would be underestimated if the inertial

terms of pore fluid and soil skeleton are neglected. The above effect from the inertial terms is overall minor which may be neglected in the engineering practice. The PD model is recommend to use if a high simulation accuracy is needed for e.g. scientific research.

(5) The presence of pile restrains the residual liquefaction adjacent to the pile surface, and the maximum liquefaction depth increases with an increase in the inserted depth of pile.

In this study, a new 3D residual model is established and the effects of the wave reflection/diffraction, inertial terms and various inserted depth of pile on the seabed residual response are investigated. Other factors, such as current, random waves (Meijers et al., 2014) and pre-shearing (Meijers and Luger, 2012) may affect the liquefaction and will be examined in future study.

Acknowledgements

This work was supported by the Fundamental Research Funds for the Central Universities [2017B15814], the International Postdoctoral Exchange Fellowship Program [20170014], National Science Foundation for Distinguished Young Scholars [Grant No. 51425901], Fundamental Research Funds for the Central Universities (2017B21514), Key Laboratory of Water-Sediment Sciences and Water Disaster Prevention of Hunan Province (2018SS02), Natural Science Foundation of Jiangsu Province [Grant No. BK20161509], Open Foundation of State Key Laboratory of Hydrology-Water Resources and Hydraulic Engineering, Hohai University [Project No:

2016491011] and National Natural Science Funds of China (41706087). The authors also give thanks to Associated Prof. David R. Fuhrman (from Technical University of Denmark) for his work on the language editing of this paper. Titi Sui also thanks Dr. Meijers (from Deltares) for providing explanations to his published paper. Reviewers' comments have greatly improved the quality of the final manuscript.

References:

Alcérreca-Huerta, J.C., Oumeraci, H., 2016. Wave-induced pressures in porous bonded revetments. Part II: Pore pressure just beneath the revetment and in the embankment subsoil. Coastal Engineering, 110, 76-86.

Cheng, L., Sumer, B.M., Fredsøe, J., 2001. Solutions of pore pressure build up due to progressive waves. International Journal for Numerical and Analytical Methods in Geomechanics, 25 (9), 885-907.

Cong, P., Gou, Y., Teng, B., Zhang, K., Huang, Y., 2015. Model experiments on wave elevation around a four-cylinder structure. Ocean Engineering, 96, 40-55.

De Alba, P., 1976. Sand liquefaction in large scale simple shear tests. Journal of the Geotechnical Engineering Division - ASCE, 102 (9), 909-927.

de Groot, M.B., Bolton, M.D., Foray, P., Meijers, P., Palmer, A.C., Sandven, R., Sawicki, A., Teh, T.C., 2006a. Physics of liquefaction phenomena around marine structures. Journal of Waterway, Port, Coastal, and Ocean Engineering – ASCE, 132 (4), 227-243.

de Groot, M.B., Kudella, M., Meijers, P., Oumeraci, H., 2006b. Liquefaction phenomena underneath marine gravity structures subjected to wave loads. Journal of

Waterway, Port, Coastal, and Ocean Engineering – ASCE, 132 (4), 325-335.

Duan, L.L., Jeng, D.-S., 2018. Numerical study for wave-induced oscillatory seabed response around pile foundations using OpenFOAM. International Journal of Offshore and Polar Engineering. In press.

Duan, L.L., Jeng, D.-S., Wang, S.H., Zhu, B., 2018. Numerical investigation of the wave/current-induced responses of transient soil around a square mono-pile foundation. Journal of Coastal Research. In press.

European Wind Energy Associatoin, 2016. The European offshore wind industry - key trends and statistics 2015.

Fuhrman, D.R., Baykal, C., Mutlu Sumer, B., Jacobsen, N.G., Fredsøe, J., 2014. Numerical simulation of wave-induced scour and backfilling processes beneath submarine pipelines. Coastal Engineering, 94, 10-22.

Jeng, D.-S., 1997. Wave-induced seabed instability in front of a breakwater. Ocean Engineering, 24(10), 887-917.

Jeng, D.-S., 2013. Porous Models for Wave-Seabed Interactions. Springer, Heidelberg.

Jeng, D.-S., Cha, D.H., 2003. Effects of dynamic soil behavior and wave non-linearity on the wave-induced pore pressure and effective stresses in porous seabed. Ocean Engineering, 30 (16), 2065-2089.

Jeng, D.-S., Seymour, B.R., 2007. Simplified analytical approximation for pore-water pressure buildup in marine sediments. Journal of Waterway, Port, Coastal, and Ocean Engineering, 133 (4), 309-312.

Jeng, D.-S., Seymour, B.R., Li, J., 2007. A new approximation for pore pressure accumulation in marine sediment due to water waves. Int. J. Numer. Anal. Meth. 31 (1), 53-69.

Jeng, D.-S., Ye, J.H., Zhang, J.S., Liu, P.L.F., 2013. An integrated model for the wave-induced seabed response around marine structures: Model verifications and applications. Coastal Engineering, 72, 1-19.

Jeng, D.-S., Zhao, H.Y., 2015. Two - dimensional model for accumulation of pore pressure in marine sediments. Journal of Waterway, Port, Coastal, and Ocean Engineering – ASCE, 141 (3), 04014042.

Kirby, J.T., Wen, L., Shi, F.Y., 2003. FUNWAVE 2.0 fully nonlinear Boussinesq wave model on curvilinear coordinates, Newark: University of Delaware.

Kirca, V.O., Sumer, B.M., Fredsøe, J., 2013. Residual liquefaction of seabed under standing waves. Journal of Waterway, Port, Coastal, and Ocean Engineering – ASCE, 139 (6), 489-501.

Liang, B., Li, H., Lee D., 2008. Bottom shear stress under wave-current interaction. Journal of Hydrodynamics, 20(1), 88-95.

Liang, B., Wu, G., Liu, F., Fan, H., Li, H., 2015. Numerical study of wave transmission over double submerged breakwaters using non-hydrostatic wave model. Oceanologia, 57, 308-317.

Liao, C., Zhao H., Jeng, D.-S., 2015. Poro-elasto-plastic model for the wave-induced liquefaction. Journal of Offshore Mechanics and Arctic Engineering - ASME, 137 (4), 042001.

Liao, C., Tong, D., Jeng, D.-S., Zhao, H., 2018. Numerical study for wave-induced oscillatory pore pressures and liquefaction around impermeable slope breakwater heads. Ocean Engineering, 157, 364-375.

Li, J., Jeng, D.S., 2008. Response of a porous seabed around breakwater heads. Ocean Engineering, 35 (8-9), 864-886.

Li, X.J., Gao, F.P., Yang, B., 2011. Wave-induced pore pressure responses and soil liquefaction around pile foundation. International Journal of Offshore and Polar Engineering, 21 (3), 233-239.

Li, Y., Tang, T., Ong, M. C., 2017. Numerical analysis of wave-induced poro-elastic seabed response around a hexagonal gravity-based offshore foundation. Coastal Engineering, 136, 81-95.

Lin, Z., Pokrajac, D., Guo, Y., Jeng, D.-S., Tang, T., Rey, N., Zheng, J., Zhang, J., 2017. Investigation of nonlinear wave-induced seabed response around mono-pile foundation. Coastal Engineering, 121, 197-211.

Liu, B., Jeng, D.-S., Ye, G., Yang, B., 2015. Laboratory study for pore pressures in sandy deposit under wave loading. Ocean Engineering, 106, 207-219.

Lu, H., 2005. The research on pore pressure response to waves in sandy seabed. Master Thesis, Technical University of Changsha.

Madsen, O.S., 1978. Wave-induced pore pressures and effective stresses in a porous bed. Géotechnique, 28 (4), 377-393.

McDougal, W.G., Tsai, Y.T., Liu, P.L.F., Clukey, E.C., 1989. Wave-induced pore water pressure accumulation in marine soils. International Journal for Numerical and Analytical Methods in Geomechanics – ASME, 111 (1), 1-11.

Meijers, P., Luger, D., 2012. On the Modelling of Wave-induced Liquefaction, Taking Into Account the Effect of Preshearing. Preeding of 22^{th} International Society of Offshore and Polar Engineers, Rhodes, Greece.

Meijers, P., Raaijmakers, T., Luger, D., 2014. The effect of a random wave field on wave induced pore pressure generation. Preeding of 24^{th} International Ocean and Polar Engineering Conference. International Society of Offshore and Polar Engineers, Busan, Korea.

Mizutani, N., Mostafa, A.M., Iwata, K., 1998. Nonlinear regular wave, submerged breakwater and seabed dynamic interaction. Coastal Engineering, 33 (2), 177-202.

Mattioli, M., Alsina, J.M., Mancinelli, A., Miozzi, M., Brocchini, M., 2012. Experimental investigation of the nearbed dynamics around a submarine pipeline laying on different types of seabed: The interaction between turbulent structures and particles. Advances in water resources, 48, 31-46.

Pietruszczak, S., Pande, G., 1996. Constitutive relations for partially saturated soils containing gas inclusions. Journal of geotechnical engineering – ASCE, 122 (1), 50-59.

Qi, W.G., Gao, F.P., 2014. Physical modeling of local scour development around a large-diameter monopile in combined waves and current. Coastal Engineering, 83 (83), 72-81.

Qi, W.-G., Gao, F.-P., 2018. Wave induced instantaneously-liquefied soil depth in a non-cohesive seabed. Ocean Engineering, 153, 412-423.

Sassa, S., Sekiguchi, H., 1999. Wave-induced liquefaction of beds of sand in a centrifuge. Géotechnique, 49 (5), 621-638.

Seed, H.B., Rahman, M.S., 1978. Wave - induced pore pressure in relation to ocean floor stability of cohesionless soils. Marine Georesources & Geotechnology, 2, 123-150.

Sekiguchi, H., Kita, K., Okamoto, O., 1995. Response of poro-elastoplastic beds to standing waves. Soils Foundation, 35 (3), 31-42.

Shi, F., Dalrymple, R.A., Kirby, J.T., Chen, Q., Kennedy, A., 2001. A fully nonlinear Boussinesq model in generalized curvilinear coordinates. Coastal Engineering, 42 (4), 337-358.

Smith, A.W.S., Gordon, A.D., 1983. Large breakwater toe failures. Journal of Waterway, Port, Coastal, and Ocean Engineering – ASCE, 109 (2), 253-255.

Smits, F., Andersen, K., Gudehus, G., 1978. Pore pressure generation. Proceedings of the Int. Symposium on Soil Mechanics Research and Foundation Design for the Oosterschelde Storm Surge Barrier, the Netherlands.

Sui, T., Zhang, C., Guo, Y., Zheng, J., Jeng, D.-S., Zhang, J., Zhang, W., 2016. Three-dimensional numerical model for wave-induced seabed response around mono-pile. Ships and Offshore Structures, 11 (6), 667-678.

Sui, T., Zheng, J., Zhang, C., Jeng, D.-S., Zhang, J., Guo, Y., He, R., 2017. Consolidation of unsaturated seabed around an inserted pile foundation and its effects on the wave-induced momentary liquefaction. Ocean Engineering, 131, 308–321.

Sumer, B.M., 2014. Liquefaction Around Marine Structures. World Scientific Publishing, Singapore.

Sumer, B.M., Fredsøe, J., Christensen, S., Lind, M.T., 1999. Sinking/floatation of pipelines and other objects in liquefied soil under waves. Coastal Engineering, 38 (2), 53-90.

Sumer, B.M., Kirca, V.S.O., Fredsøe, J., 2012. Experimental validation of a mathematical model for seabed liquefaction under waves. International Journal of Offshore and Polar Engineering, 133-141.

Sumer, B.M., Truelsen, C., oslash, Freds, Oslash, R., 2006. Liquefaction around pipelines under Waves. Journal of Waterway, Port, Coastal, and Ocean Engineering – ASCE, 132 (4), 266-275.

Tong, D., Liao, C., Jeng, D.-S., Wang, J., 2018. Numerical study of pile group effect on wave-induced seabed response. Applied Ocean Research, 76, 148-158.

Ulker, M.B.C., Rahman, M.S., Guddati, M., 2010. Wave-induced dynamic response and instability of seabed around caisson breakwater. Ocean Engineering 37 (17), 1522-1545.

Ulker, M.B.C., Rahman, M.S., 2009. Response of saturated and nearly saturated porous media: Different formulations and their applicability. International journal for numerical and analytical methods in geomechanics, 33(5), 633-664.

Verruijt, A., 1969. Elastic storage of aquifers. Flow through porous media. Academic Press, Massachusetts.

Wei, G., Kirby, J.T., Grilli, S.T., Subramanya, R., 1995. A fully nonlinear Boussinesq model for surface waves. Part 1. Highly nonlinear unsteady waves. Journal of Fluid Mechanics, 294 (13), 71-92.

Yamamoto, T., Koning, H.L., Sellmeijer, H., Hijum, E.V., 1978. On the response of a poro-elastic bed to water waves. Journal of Fluid Mechanics, 87 (1), 193-206.

Ye, J.H., 2012. 3D liquefaction criteria for seabed considering the cohesion and friction of soil. Appllied Ocean Research, 37, 111-119.

Ye, J.H., Jeng, D.-S., 2011. Effects of bottom shear stresses on the wave-induced dynamic response in a porous seabed: PORO-WSSI (shear) model. Acta Mechanica Sinica, 27(6), 898–911.

Ye, J.H., Jeng, D.-S., Wang, R., Zhu, C., 2015. Numerical simulation of the wave-induced dynamic response of poro-elastoplastic seabed foundations and a composite breakwater. Appllied Ocean Research, 39 (1), 322-347.

Zen, K., Yamazaki, H., 1990. Oscillatory pore pressure and liquefaction in seabed induced by ocean waves. Soils Foundation, 30 (4), 161-179.

Zhang, C., Sui, T., Zheng, J., Xie, M., Nguyen, V.T., 2016. Modelling wave-induced 3D non-homogeneous seabed response. Appllied Ocean Research, 61, 101-114.

Zhang, C., Zhang, Q., Wu, Z., Zhang, J., Sui, T., Wen, Y., 2015. Numerical study on effects of the embedded monopile foundation on local wave-induced porous seabed response. Mathematical Problems in Engineering, 501, 184621.

Zhang, C., Zhang, Q., Zheng, J., Demirbilek, Z., 2017. Parameterization of nearshore wave front slope. Coastal Engineeing, 127, 80-87.

Zhang, J., Zhang, Y., Jeng, D.-S., Liu, P., Zhang, C., 2014. Numerical simulation of wave-current interaction using a RANS solver. Ocean Engineering, 75, 157-164.

Zhang, Q., Zhou, X.-L., Wang, J.-H., Guo, J.-J., 2017. Wave-induced seabed response around an offshore pile foundation platform. Ocean Engineering, 130, 567-582.

Zhang, S., Jia, Y., Zhang, Y., Shan, H., 2018. Influence of seepage flows on the erodibility of fluidized silty sediments: parameterization and mechanisms. Journal of Geophysical Research: Oceans, 123(5), 3307-3321.

Zhao, H.Y., Jeng, D.-S., 2016. Accumulated pore pressures around submarine pipeline buried in trench layer with partial backfills. Journal of Engineering Mechanics - ASCE, 142 (7), 04016042.

Zhao, H.Y., Jeng, D.-S., Liao, C.C., Zhu, J.F., 2017a. Three-dimensional modeling of wave-induced residual seabed response around a mono-pile foundation. Coastal Engineeing, 128, 1-21.

Zhao, H.Y., Jeng, D.-S., Zhang, J.S., Liao, C.C., Zhang, H.J., Zhu, J.F., 2017b. Numerical study on loosely deposited foundation behavior around a composite breakwater subject to ocean wave impact. Engineering Geology, 227, 121-138.

Zhang, W., Cao, Y., Zhu, Y., Zheng, J.H., Ji, X.M., Xu, Y.W., Wu, Y., Hoitink, A.J.F., 2018. Unravelling the causes of tidal asymmetry in deltas. Journal of Hydrology, 564, 588-604.

Zheng, J., Zhang, C., Demirbilek, Z., Lin, L., 2014. Numerical study of sandbar migration under wave-undertow interaction. Journal of Waterway, Port, Coastal, and Ocean Engineering – ASCE, 140 (2), 146-159.

Zhou, X.L., Zhang, J., Lv, H.J., Chen, J.J., Wang, J.H., 2018. Numerical analysis on random wave-induced porous seabed response. Marine Georesources & Geotechnology, 36(8), 974-985.

Zienkiewicz, O., Chang, C., Bettess, P., 1980. Drained, undrained, consolidating and dynamic behaviour assumptions in soils. Géotechnique, 30 (4), 385-395.

Table lists:

Table 1. Parameters used in the first application case

Parameters		Notations	Magnitudes	Units
Pile foundation	Radius	R_p	2.5	m
	Young's modulus	E_p	10	GPa
	Poisson's ratio	μ_p	0.25	-
	Pile length	l	14	m
	Embedded depth	de	8	m
Wave	Depth	d	4	m
	Density	ρ_f	1000	Kg/m^3
	Wave height	H	0.2-0.4	m
	Wave period	T	4-8	s
Seabed	Permeability	k	2×10^{-4}-4×10^{-5}	m/s
	Porosity	n	0.425	-
	Relative density	D_r	0.28-0.32	-
	Saturation degree	S_r	0.98-0.992	-
	Poisson's ratio	μ_s	0.35	-
	Young's modulus	E_s	5×10^{6}-7×10^{7}	Pa

Table 2. Parameters used in the second application case

Parameters		Notations	Magnitudes	Units
Pile foundation	Radius	R_p	1.5	m
	Young's modulus	E_p	10	GPa
	Poisson's ratio	μ_p	0.3	-
	Pile length	l	24	m
	Embedded depth	de	0-12	m
Wave	Depth	d	8	m
	Density	ρ_f	1000	Kg/m^3
	Wave height	H	3	m
	Wave period	T	8	s
Seabed	Permeability	k	1×10^{-5}	m/s
	Porosity	n	0.3	-
	Relative density	D_r	0.28	-
	Saturation degree	S_r	0.992	-
	Poisson's ratio	μ_s	0.3	-
	Young's modulus	E_s	1.6×10^{8}	Pa

Figure

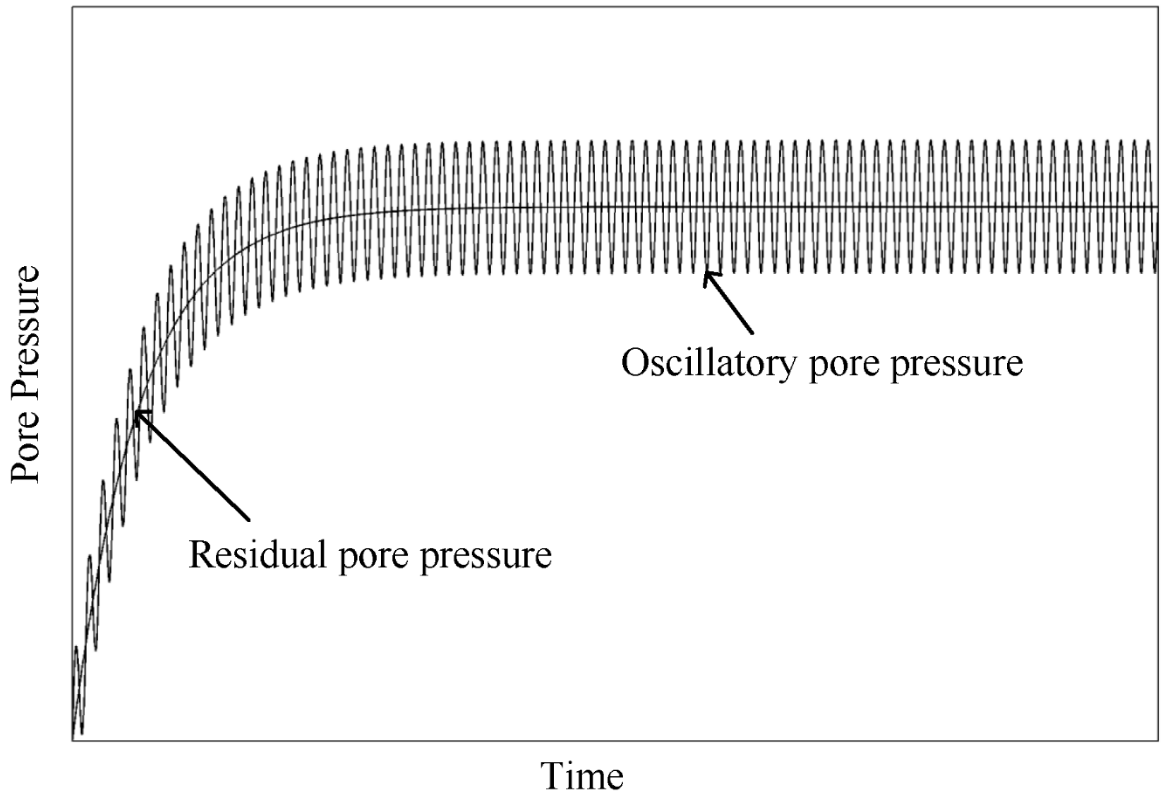

Fig. 1 Mechanisms of wave-induced pore pressures (not to scale)

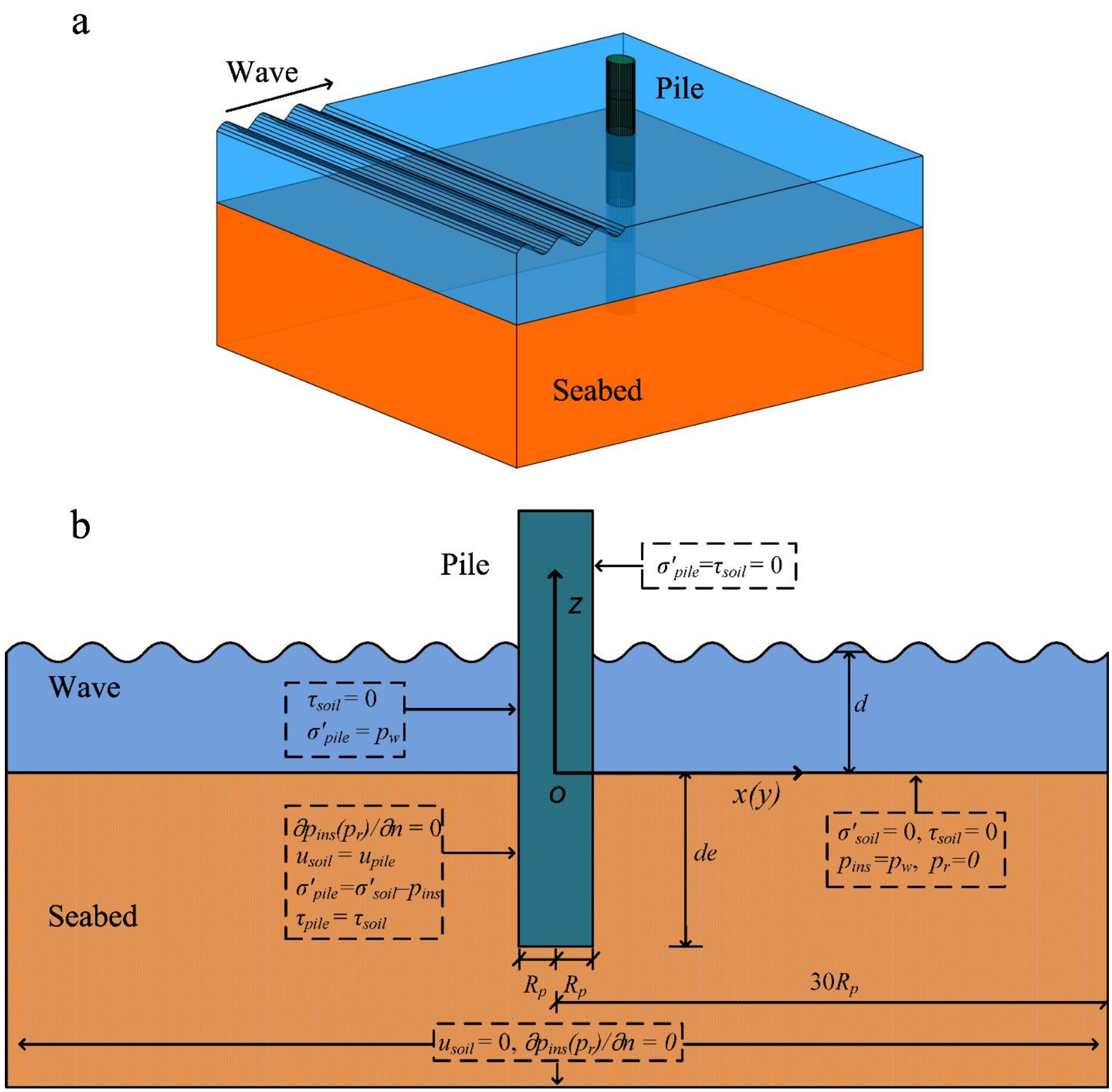

Fig. 2 (a) 3D Sketch and (b) boundary conditions of the present model in which d is the water depth, de is the embedded depth of the pile, R_p is the pile radius.

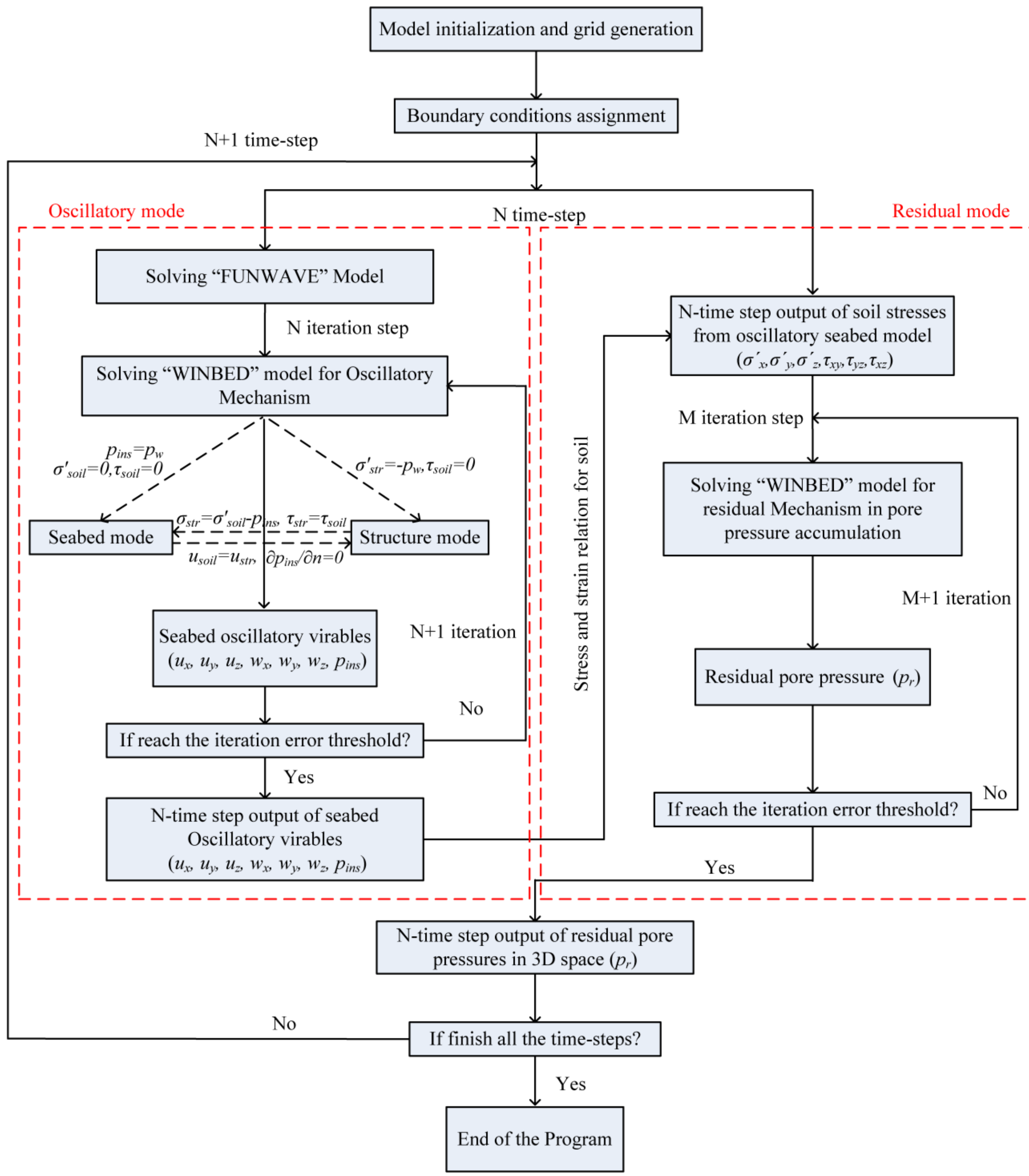

Fig. 3 Integrating procedure of the present numerical model.

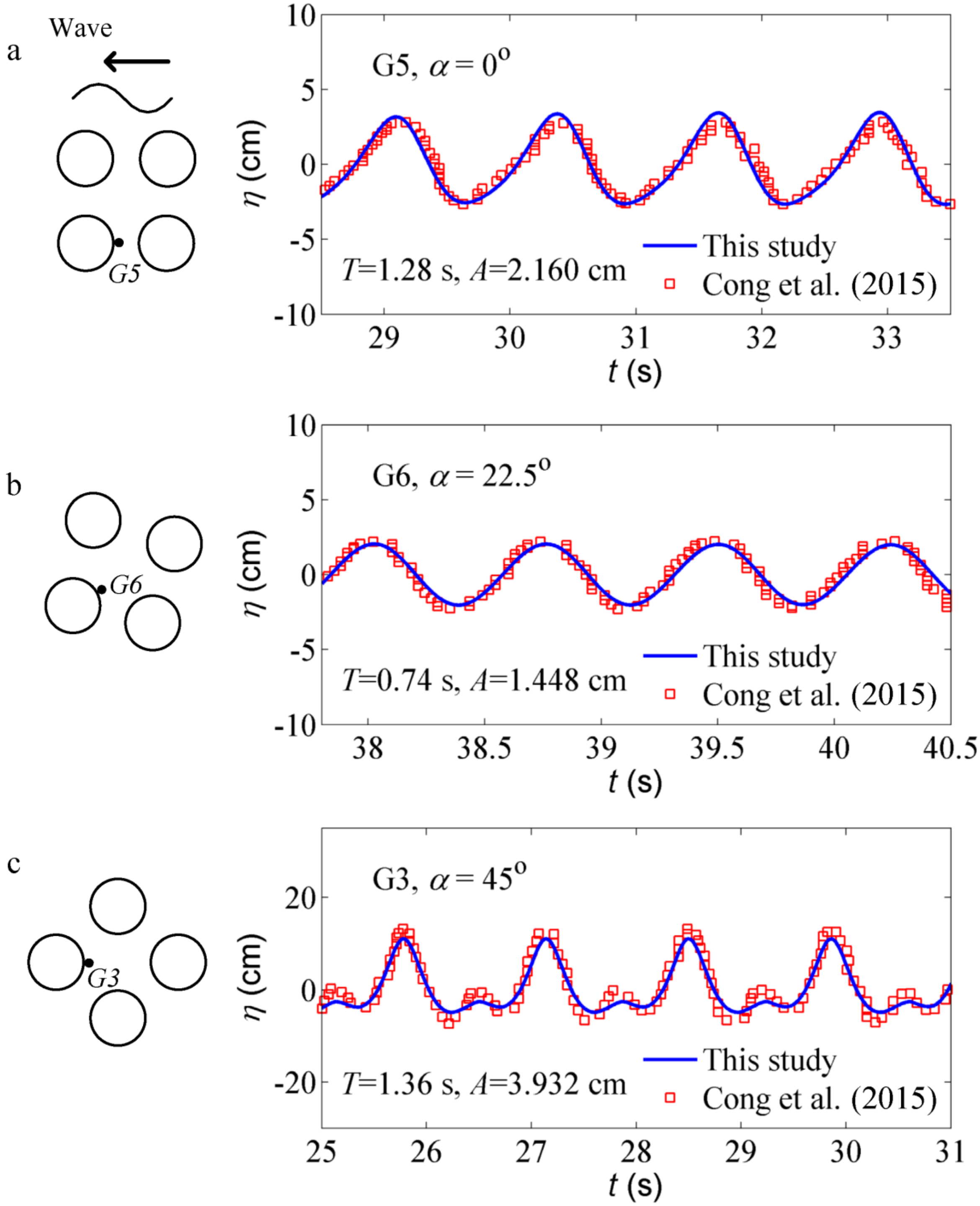

Fig. 4 Comparison of simulated (this study) and measured wave elevations (Cong et al. 2015) considering wave-pile interactions

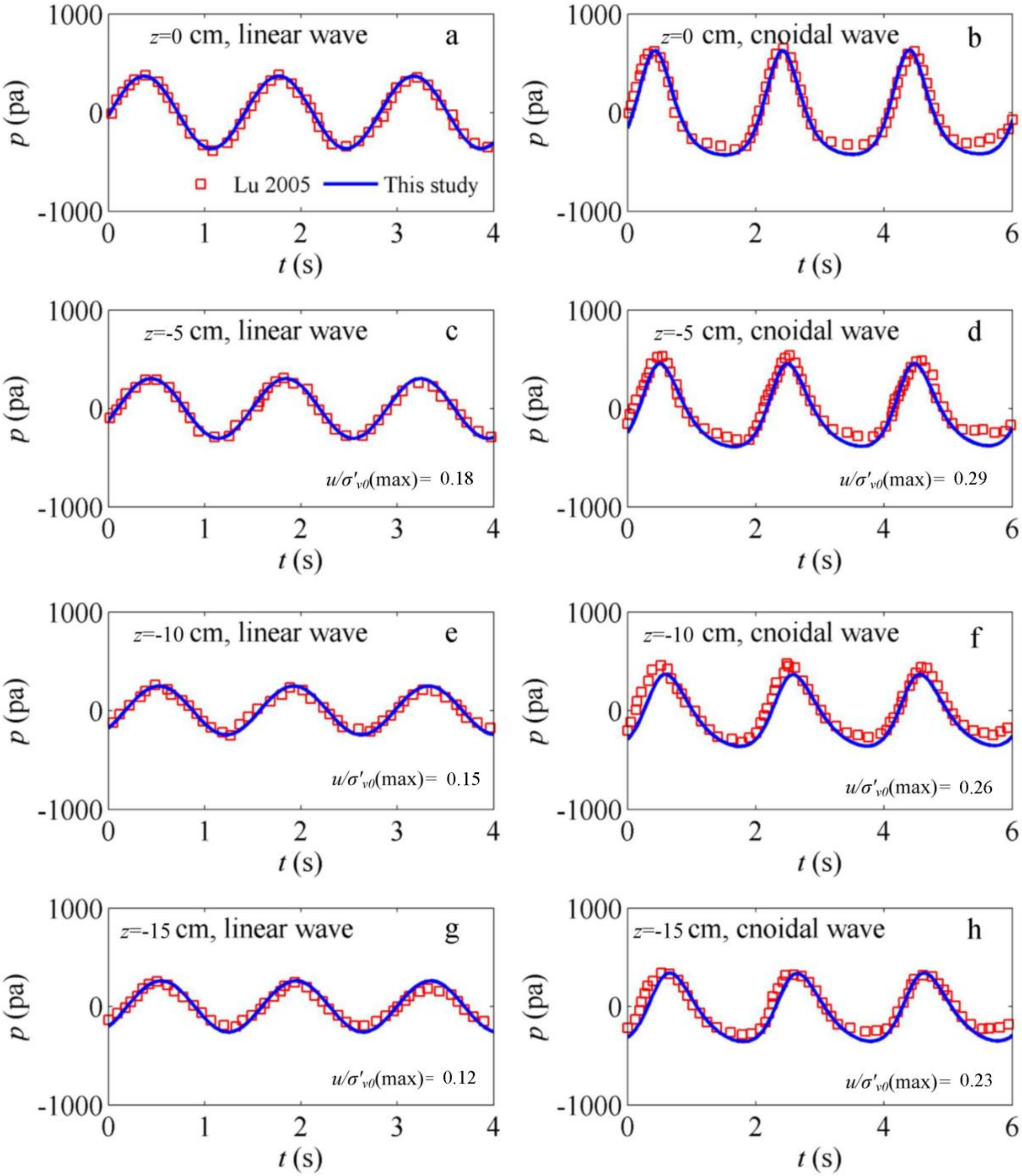

Fig. 5 Comparison of simulated (this study) and measured (Lu, 2005) wave induced dynamic pore water pressure at different soil depth for (a, c, e, g) linear wave and (b, d, f, h) cnoidal wave.

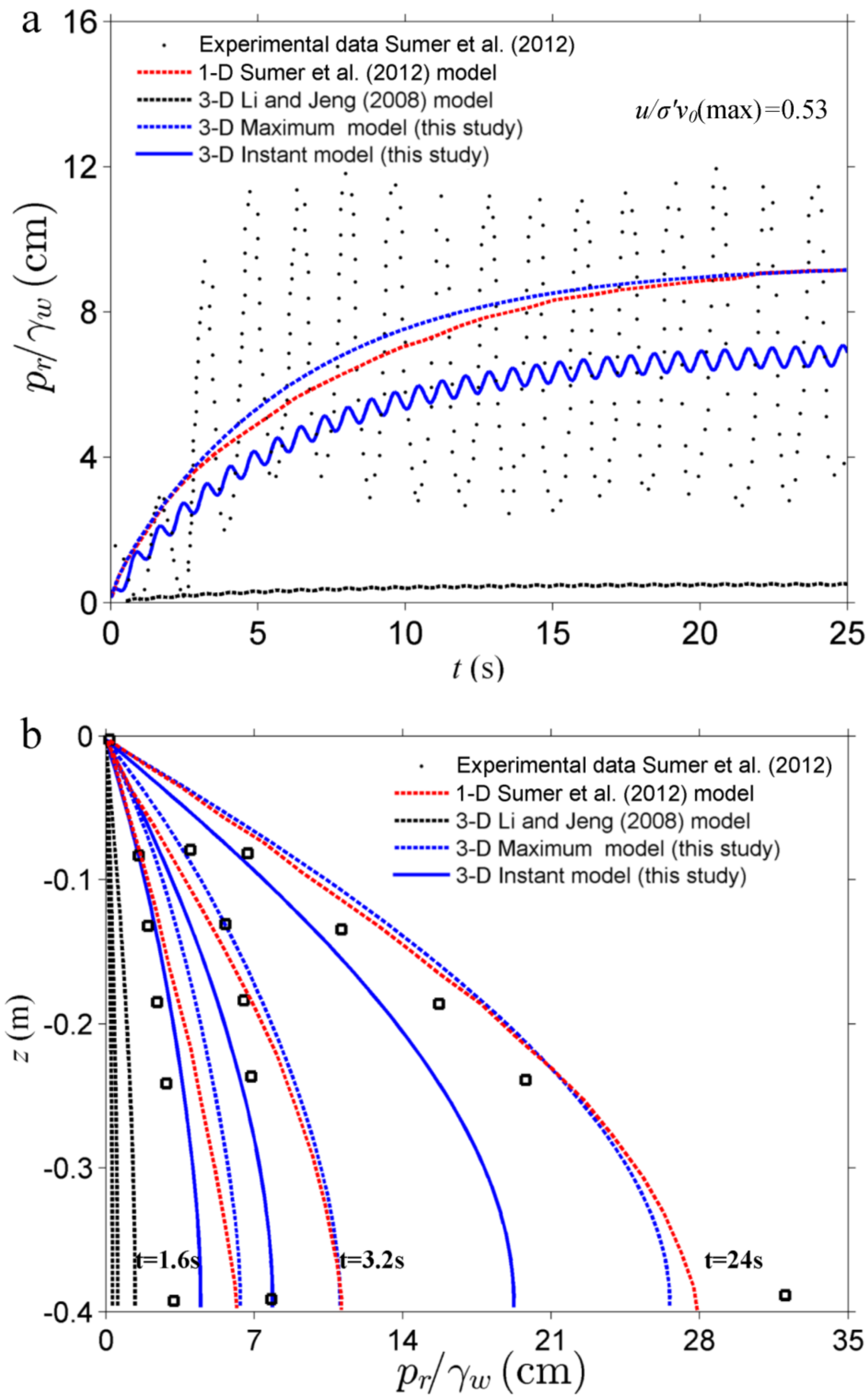

Fig. 6 Comparisons of simulated (Li and Jeng (2008), Sumer et al., (2012), this study) and measured (Sumer et al., (2012)) pore pressure build-up within a silt seabed (the oscillatory part of pore pressure is manually removed here).

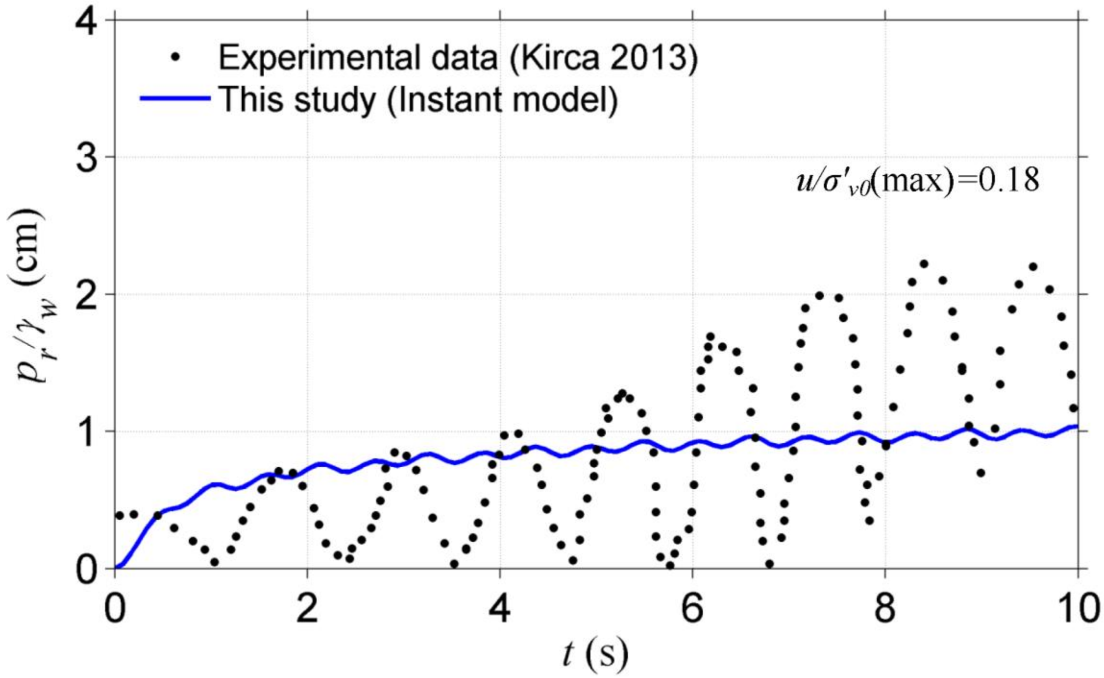

Fig. 7 Comparisons of simulated (this study) and measured (Kirca, 2013) pore pressure build-up within a silt seabed with a standing wave (the oscillatory part of pore pressure is manually removed here).

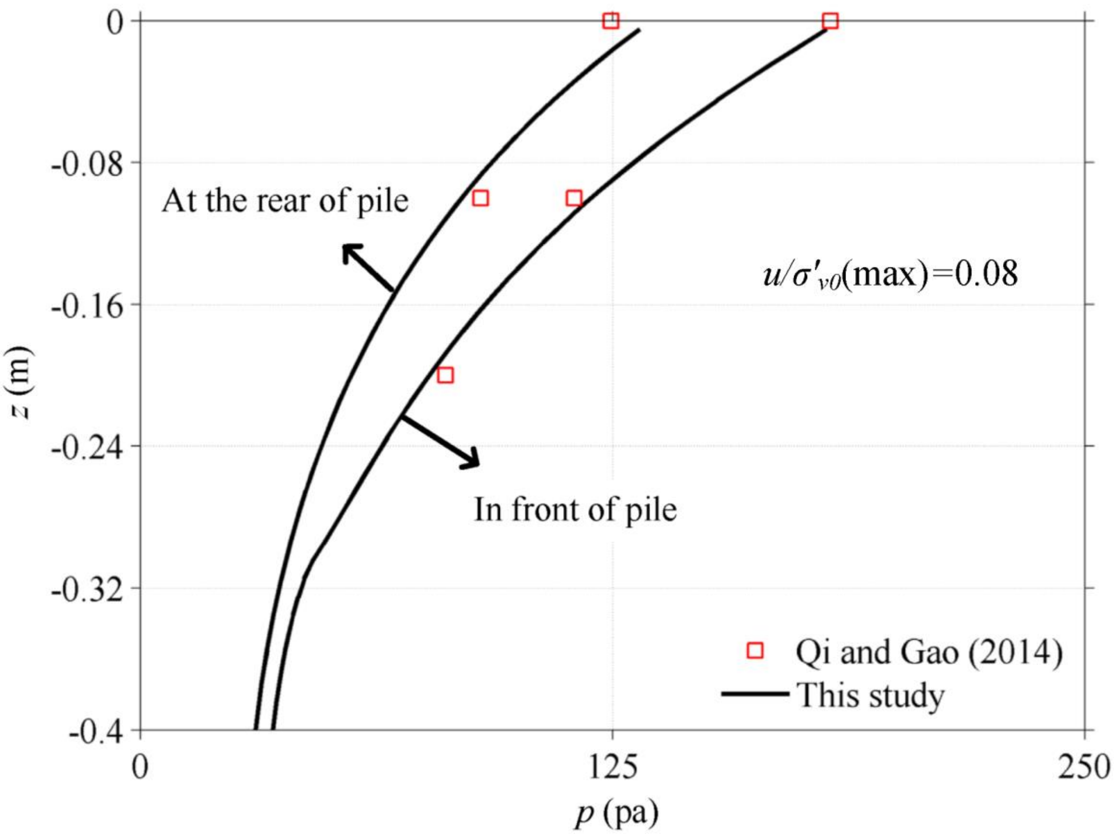

Fig. 8 Comparisons of simulated (this study) and measured (Qi and Gao, 2014) pore pressure vertical distributions around a mono-pile foundation.

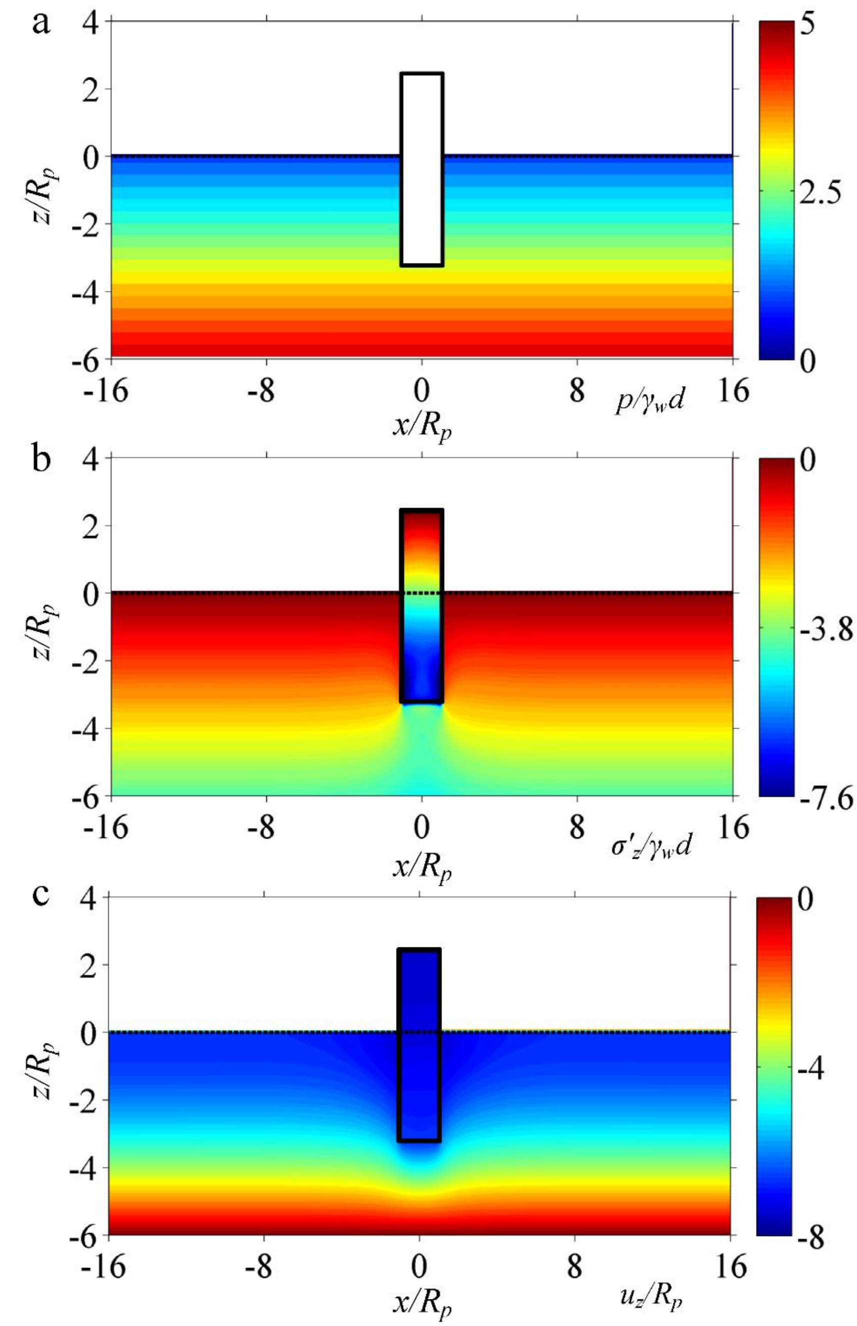

Fig. 9 The consolidation state of seabed for (a) pore pressure, (b) effective stress and (c) subsidence in the vicinity of a mono-pile (H=0 m, k=2×10^{-5} m/s, de=8 m).

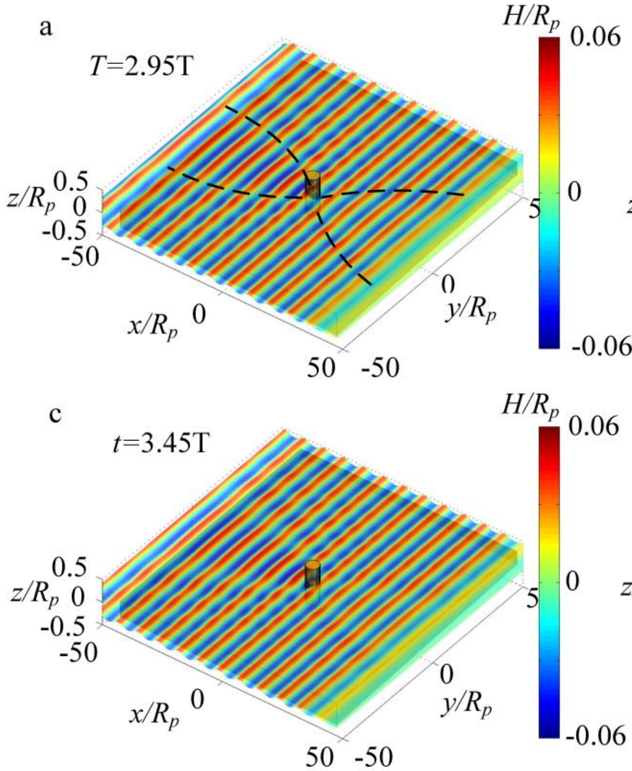

Fig. 10 3D distribution of wave surface elevation around a mono-pile for (a) t=2.95T, (b) t=3.2T, (c) t=3.45T and t=3.70T. (H=0.2 m)

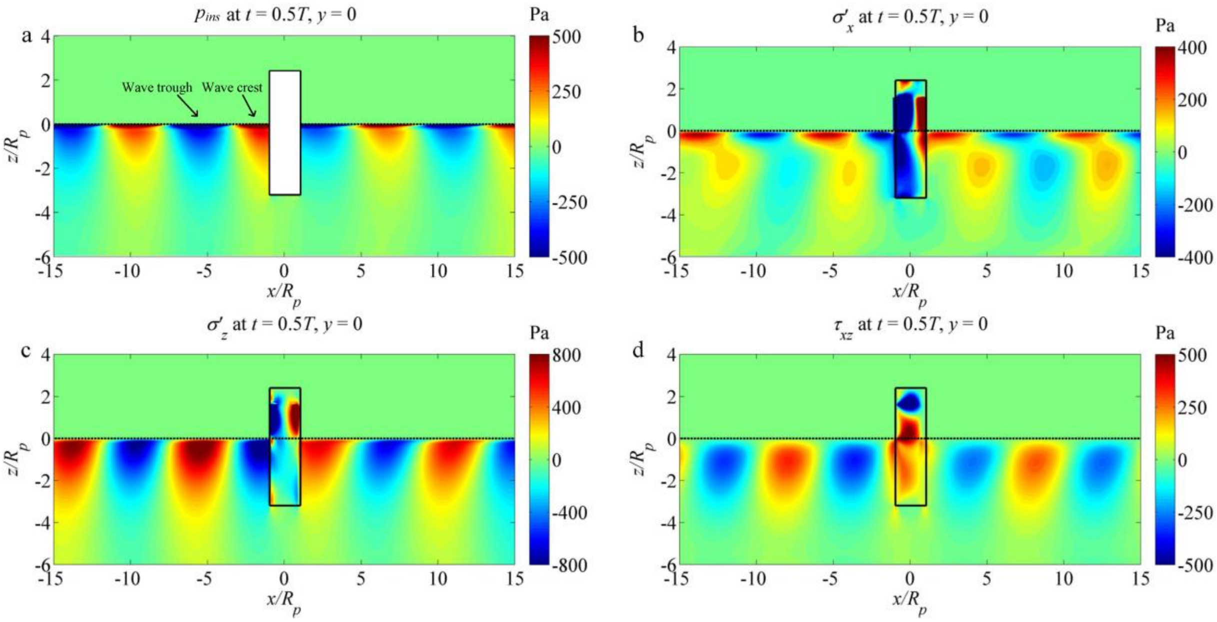

Fig. 11 Distribution of (a) oscillatory pore pressure (p_{ins}), (b) horizontal effective stress (σ'_x), (c) vertical effective stress (σ'_x) and (d) shear stress (τ_{xz}) around a mono-pile for t=0.5T (H=0.4 m)

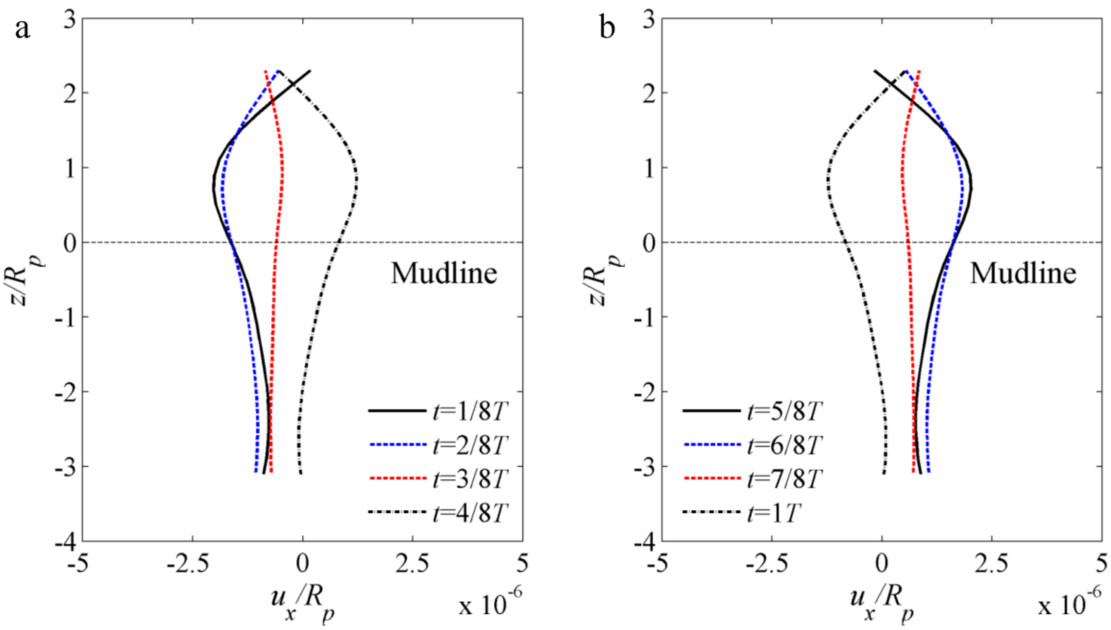

Fig. 12 Cyclic horizontal displacements of the pile (u_x) under the dynamic wave loading for one wave period (H=0.4 m)

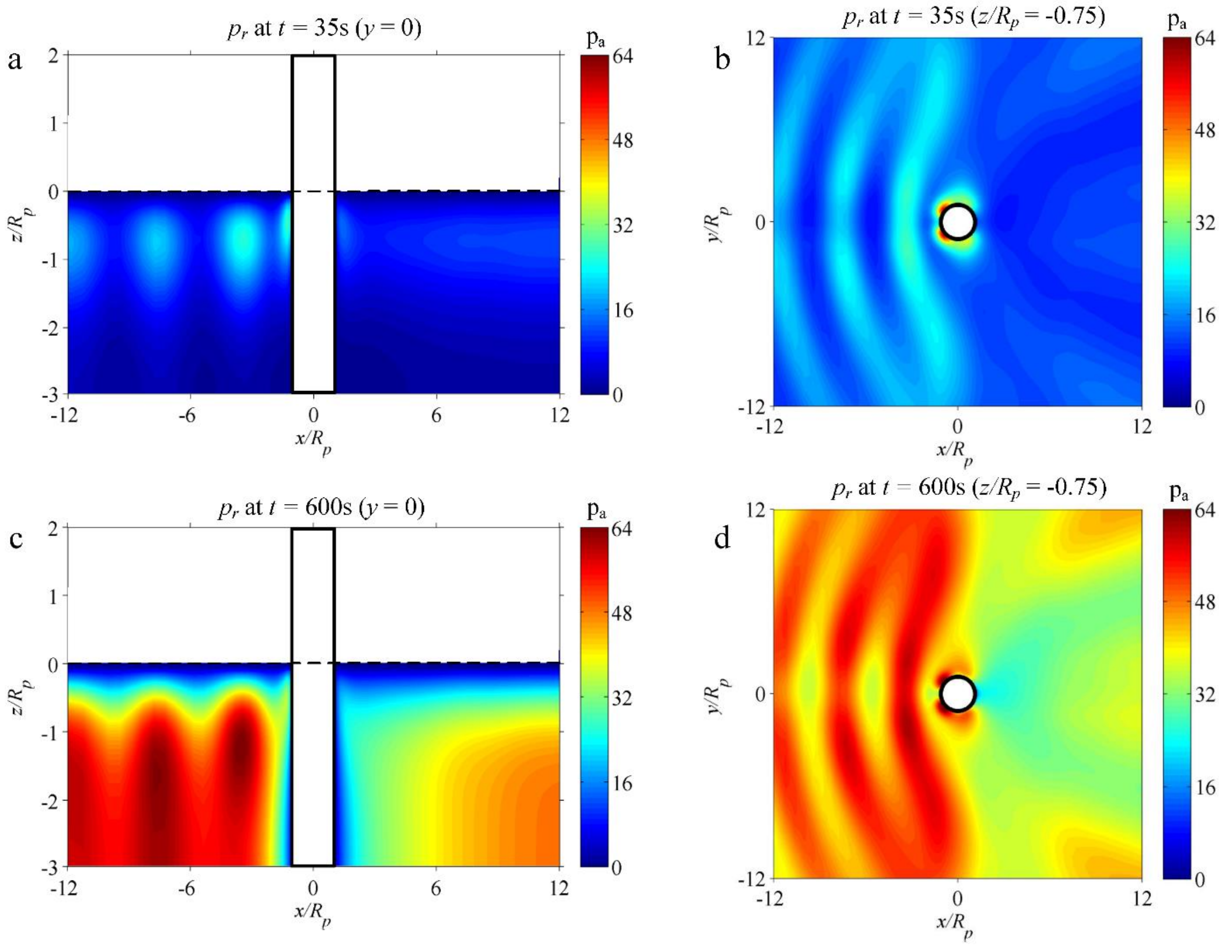

Fig. 13 3D temporal and spatial features of the accumulated pore pressure (p_r) around a mono-pile for (a) p_r at t=35 s in x-z section (y/R_p=0), (b) p_r at t=35 s in x-y section (z/R_p=-0.75), (c) p_r at t=600 s in x-z section (y/R_p=0) and (d) p_r at t=600 s in x-y section (z/R_p=-0.75). (H=0.2 m, k=1×10^{-5} m/s, D_r=0.28, de=8 m)

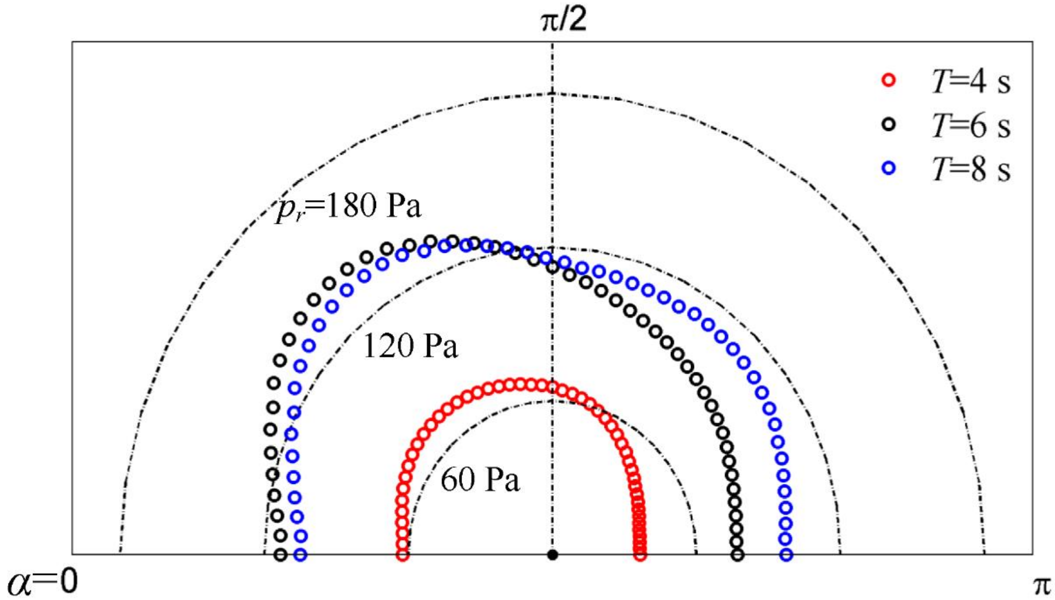

Fig. 14 Effects of wave periods (T) on residual pore pressure (x-y plane) in the vicinity of a mono-pile foundation. (H=0.2 m, k=1×10^{-5} m/s, D_r=0.28, z/R_p=-1, S/R_p=1, de=8 m, t=600 s)

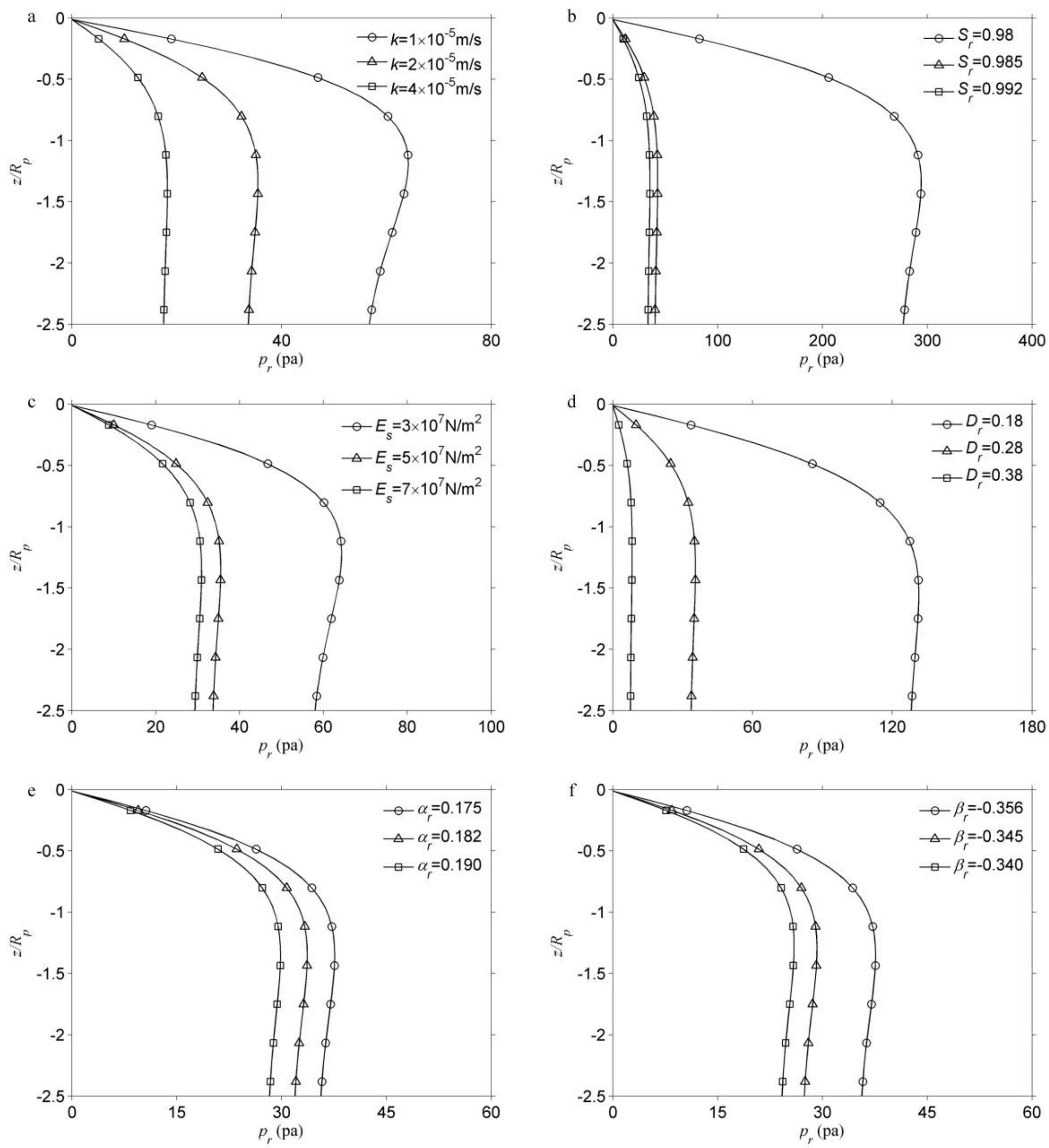

Fig. 15 Vertical distribution of the residual pore pressures (t=600 s, T=4 s, H=0.2 m, d=4 m) for (a) different seabed permeability k (S_r=0.992, E_s=5×10^7 N/m^2, D_r=0.28), (b) Saturation degree S_r (k = 2×10^{-5} m/s, E_s=5×10^7 N/m^2, D_r=0.28), (c) Young's modulus E_s (k = 2×10^{-5} m/s, S_r=0.992, D_r=0.28), (d) relative density D_r (k=2×10^{-5} m/s, S_r=0.992, E_s=5×10^7 N/m^2), (e) coefficient α_r (S_r=0.992, E_s=5×10^7 N/m^2, β_r=-0.356) and (f) coefficient β_r=-0.356 (S_r=0.992, E_s=5×10^7 N/m^2, α_r=0.175).

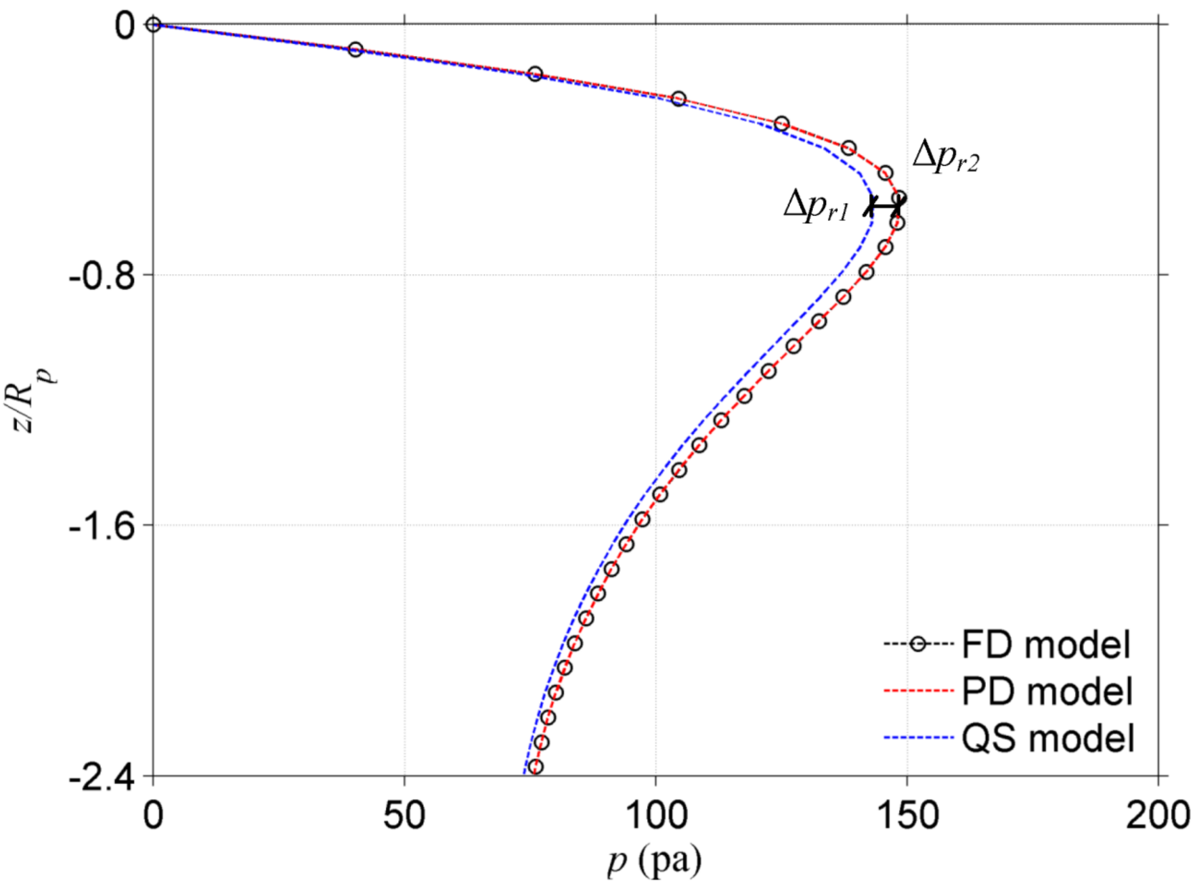

Fig. 16 Vertical distributions of the residual pore pressure simulated by Fully-Dynamic model, Partial-Dynamic model and Quasi-Static model. (H=0.4 m, k=2×10^{-4} m/s, D_r=0.28, de=8 m, E_s=5×10^{6} N/m^{2})

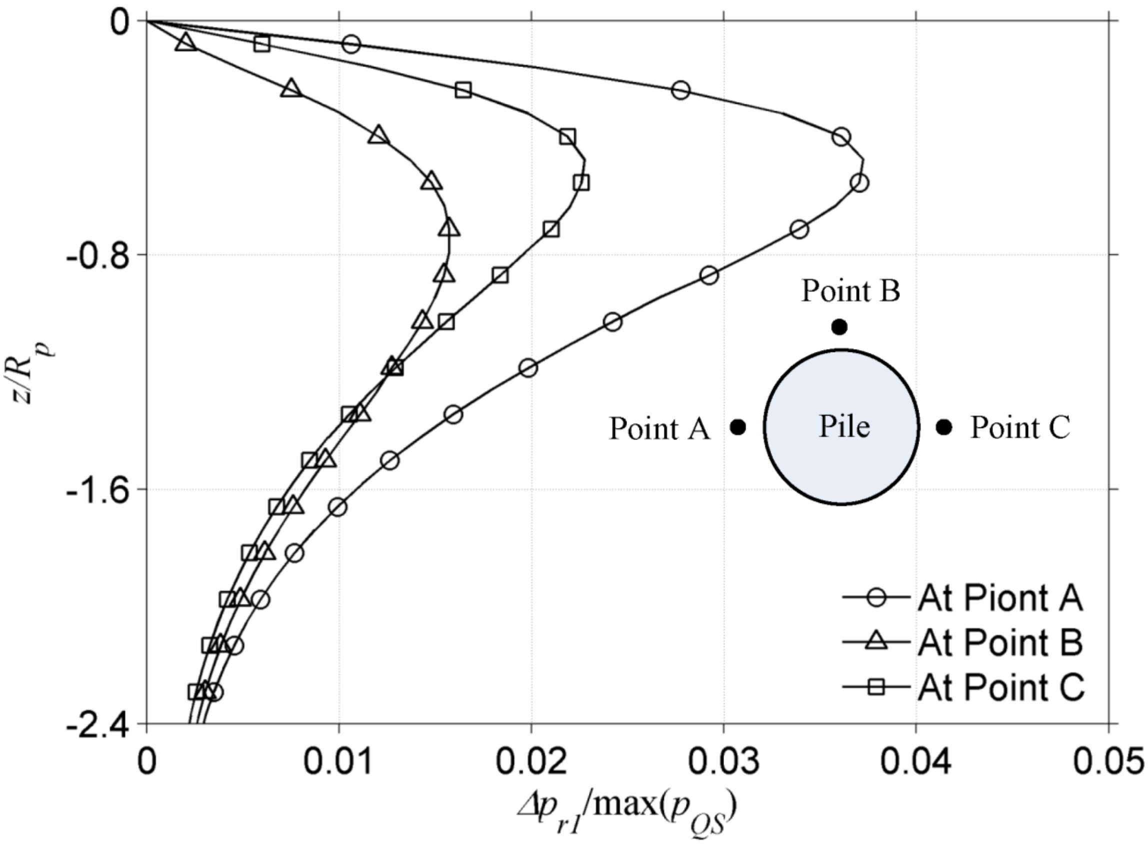

Fig. 17 Vertical distribution of pore pressure discrepancy (Δp_{r1}/max(p_{QS})) in front (Point A), at sides (Point B) and at rear (Point C) of a mono-pile foundation (max(p_{QS}) is the maximum pore pressure with Quasi-static model) (H=0.4 m, k=2×10^{-4} m/s, D_r=0.28, de=8 m, E_s=5×10^6 N/m^2).

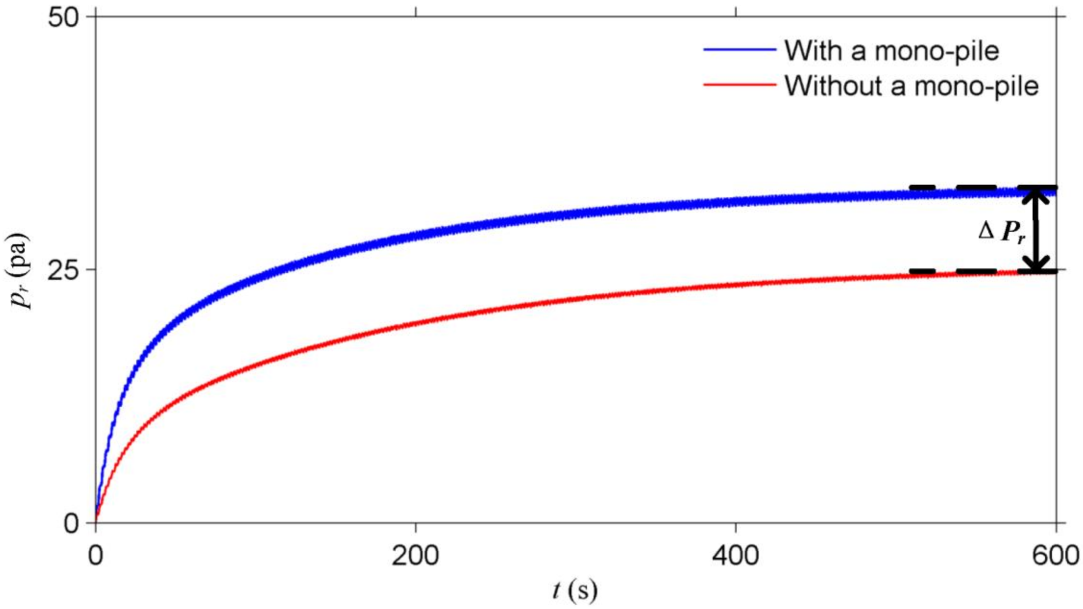

Fig. 18 Comparisons of the accumulated pore pressure with and without a mono-pile foundation at the location of x/R_p=-3.5, y/R_p=0, z/R_p=-0.83. (H=0.2 m, k=2×10^{-5} m/s, D_r=0.28, de=8 m)

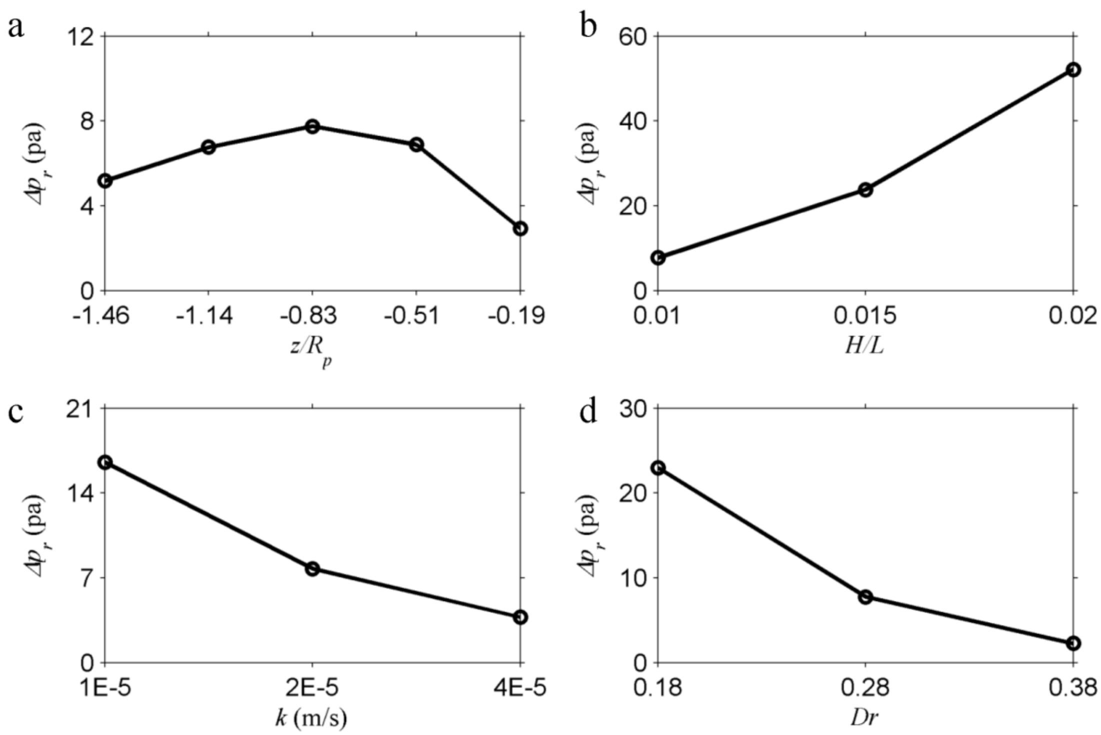

Fig. 19 Significance of mono-pile foundation against various (a) vertical locations (z) (H/L=0.01, k=2×10^{-5} m/s, D_r=0.28), (b) wave steepness (H/L) (k=2×10^{-5} m/s, D_r=0.28), (c) seabed permeability (k) (H/L=0.01, D_r=0.28) and (d) seabed relative density (D_r) (H/L=0.01, k=2×10^{-5} m/s). (de=8 m)

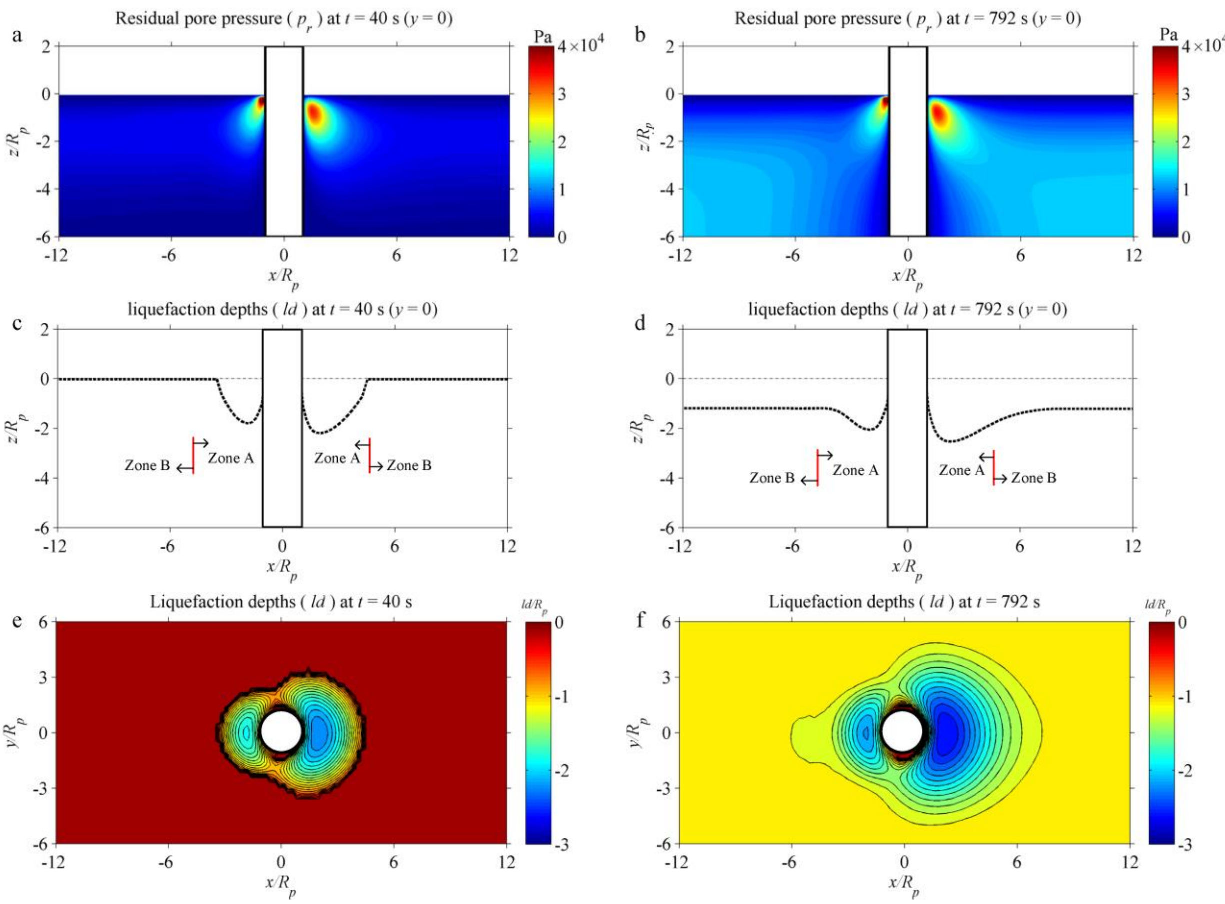

Fig. 20 Residual pore pressure (p_r) and liquefaction depth (ld in the x-z plane and x-y plane) in the vicinity of a mono-pile at t=40 s (a, c and e) and t=792 s (b, d and f) (de/R_p=8).

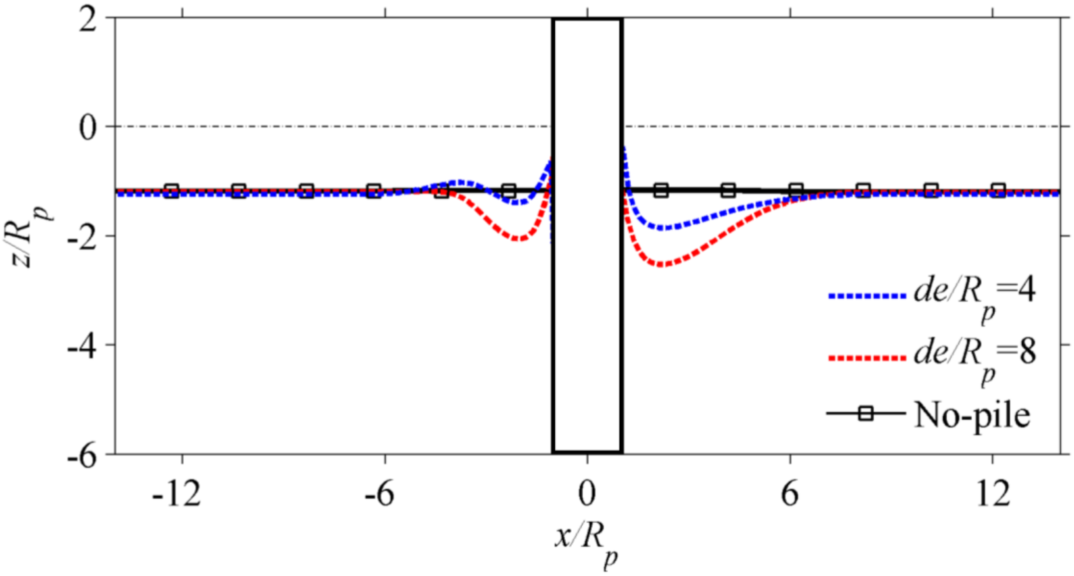

Fig. 21 Liquefaction depth (*ld*) around a mono-pile for different pile embedded depth (*de*).

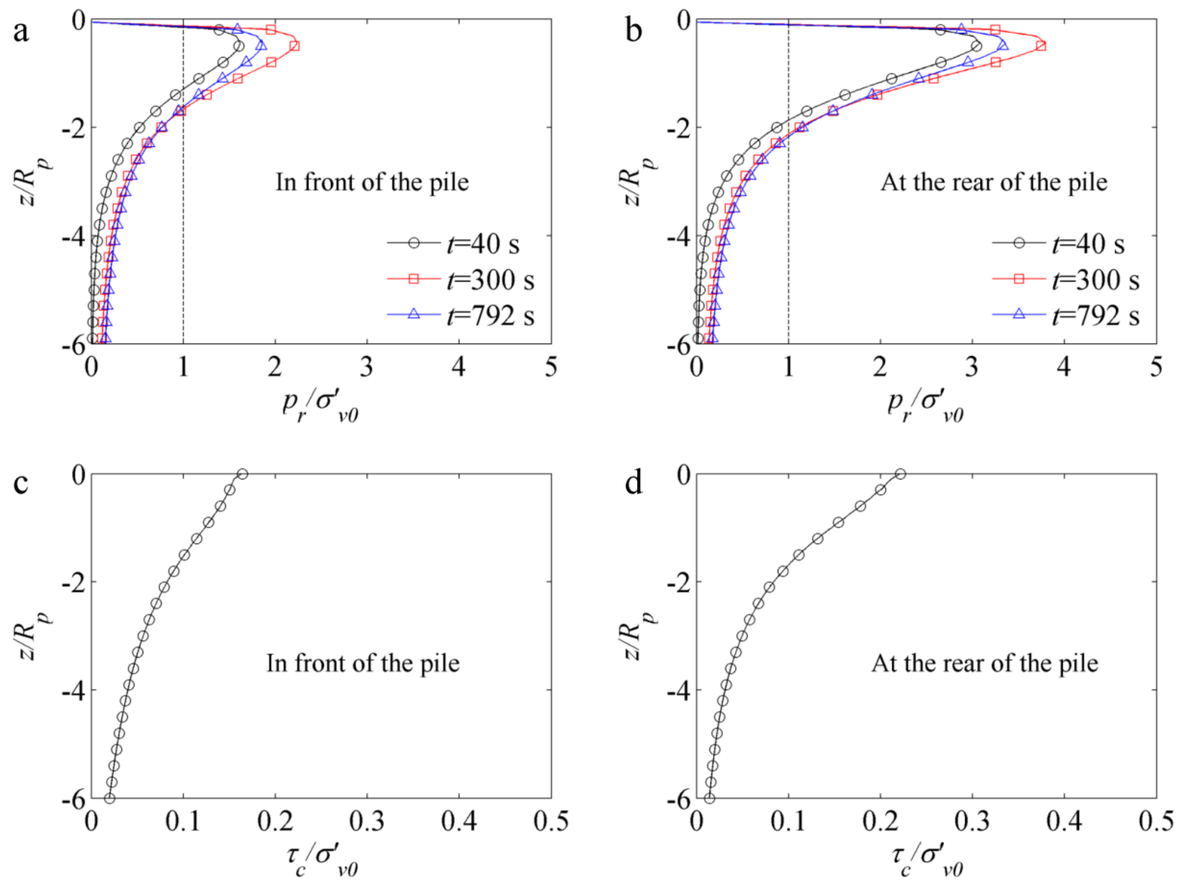

Fig. 22 The ratio of excess pore pressure u/σ'_{v0} (the fluidization degree) (a, b) as well as the relative cyclic shear stress amplitude (CSR) (c, d) in front (x/R_p=-2.5) and at the rear (x/R_p=2.5) of the mono-pile (de/R_p=8).

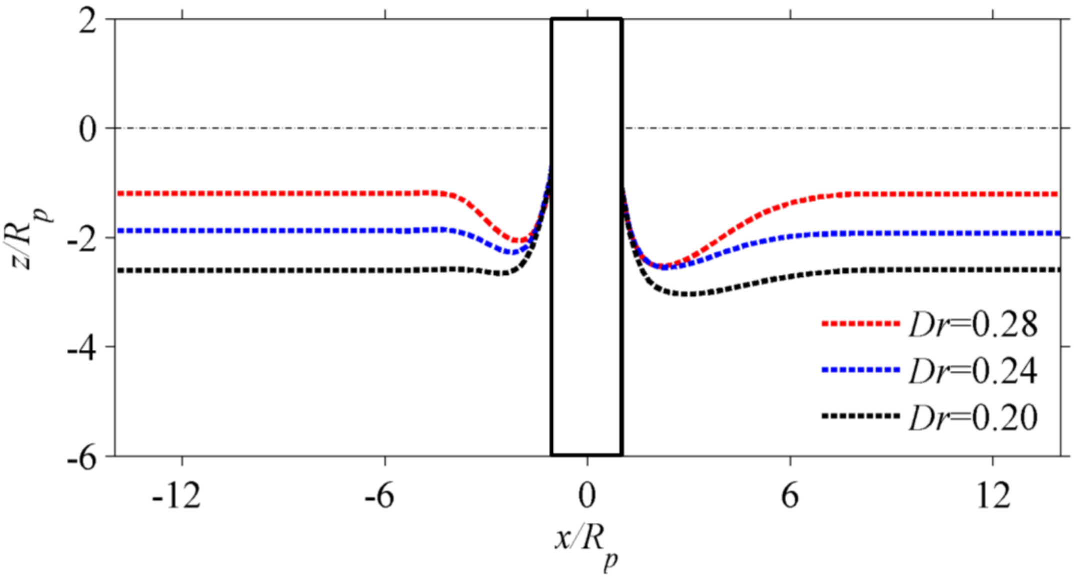

Fig. 23 Effects of soil relative density D_r on the liquefaction depth around the pile (de/R_p=8).

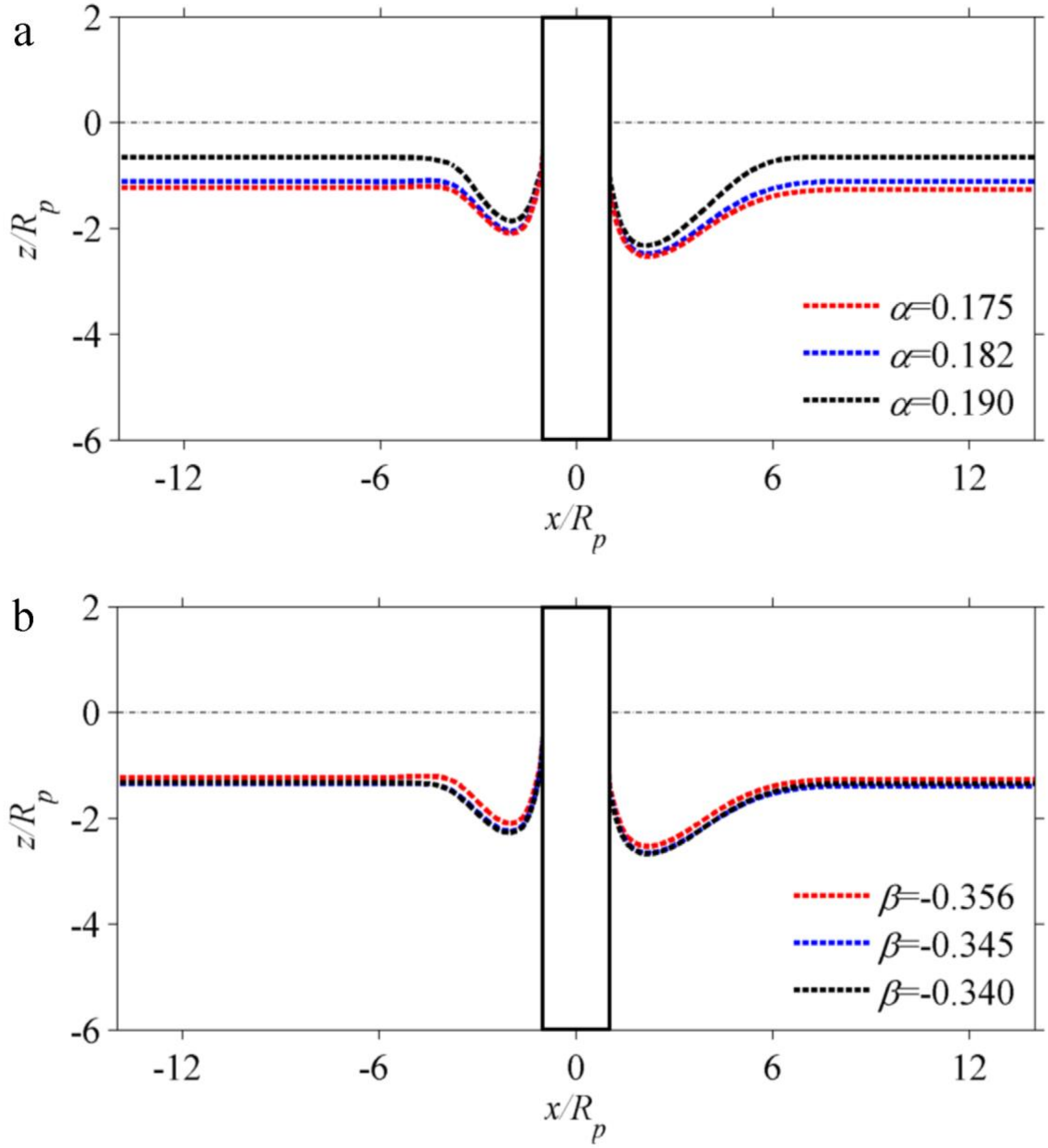

Fig. 24 Effects of (a) coefficients α_r (β_r=-0.356) and (b) coefficients β_r (α_r=0.175) on the liquefaction depth around the pile (de/R_p=8).

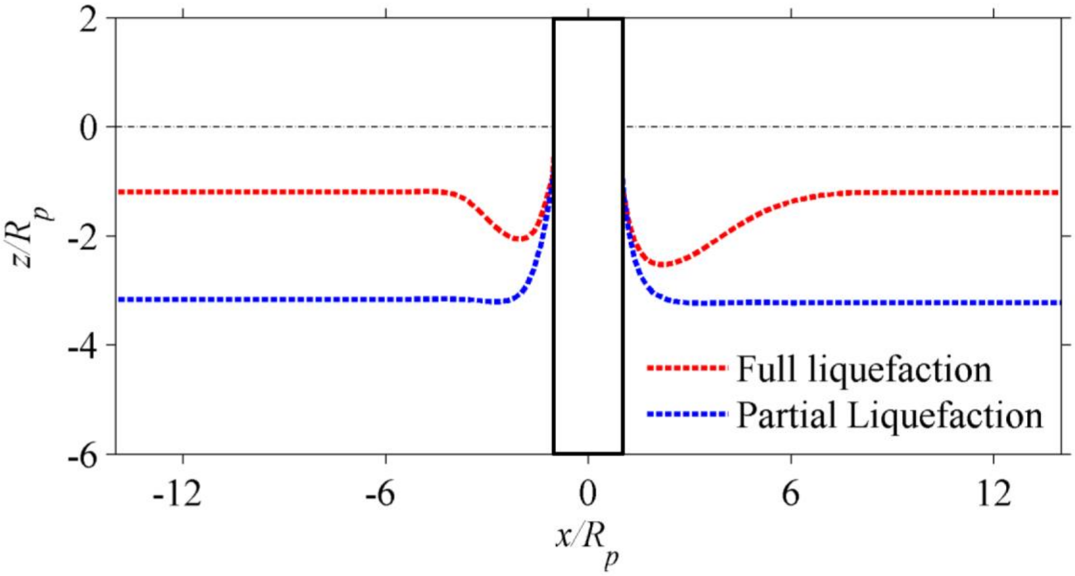

Fig. 25 Comparison of liquefaction depth with full liquefaction criteria and partial liquefaction criteria around the pile foundation (de/R_p=8).